NASA Contractor Report 165893

A Doublet Lattice Method for the Determination of Rotor Induced Empennage Vibration Airloads — Analysis Description and Program Documentation

Santu. T. Gangwani

UNITED TECHNOLOGIES RESEARCH CENTER

East Hartford, CT 06108

NASA

National Aeronautics and
Space Administration

Langley Research Center
Hampton, Virginia 23665
AC 804   827-3966

A DOUBLET LATTICE METHOD FOR THE DETERMINATION
OF ROTOR INDUCED EMPENNAGE VIBRATION AIRLOADS –
ANALYSIS DESCRIPTION AND PROGRAM DOCUMENTATION

TABLE OF CONTENTS

TABLE OF CONTENTS (Cont'd)

LIST OF FIGURES

LIST OF FIGURES (Cont'd)

LIST OF TABLES

A DOUBLET LATTICE METHOD FOR THE DETERMINATION OF ROTOR INDUCED EMPENNAGE VIBRATION AIRLOADS – ANALYSIS DESCRIPTION AND PROGRAM DOCUMENTATION[*]

SUMMARY

An efficient state-of-the-art method has been developed to determine the unsteady vibratory airloads produced by the interaction of the main rotor wake with a helicopter empennage. This method has been incorporated into a computer program, Rotor Induced Empennage Vibration Analysis (RIEVA). The program requires the main rotor wake position and the strength of the vortices located near the empennage surfaces. A nonlinear lifting surface analysis is utilized to predict the aerodynamic loads on the empennage surfaces in the presence of these concentrated vortices. The analysis has been formulated to include all pertinent effects such as suction of the interacting vortices and the shed vorticity behind the empennage surfaces. The analysis employs a stepwise solution (time domain); that is, a period corresponding to one blade passage is divided into a large number of time intervals and unsteady airloads are computed at each step. The output of the program consists of chordwise and spanwise airload distributions on the empennage surfaces. The airload distributions are harmonically analyzed and formulated for input into the Coupled Rotor/Airframe Vibration Analysis (Ref. 6). This report describes the theoretical development for the analysis, the RIEVA program documentation and output of a sample case of the program.

I. INTRODUCTION

The unsteady airloads produced by the interaction of the main rotor wake with the helicopter empennage (horizontal stabilizer/vertical fin) can be a major source of vibratory loads on a helicopter (Ref. 1). An efficient state-of-the-art method has been developed to determine these unsteady airloads due to the passage of concentrated main rotor wake vortices in the vicinity of the empennage. Since future helicopters are expected to be operating with high disk loading resulting in strong blade tip vortices in the rotor wake, the order of magnitude of these unsteady airloads will be significantly higher. As a consequence, these airloads will have to be determined in the early design and development stage to insure an efficient design. Therefore, the main purpose behind the development of this analysis is to establish an effective reliable methodology which can be utilized to analytically predict these rotor wake induced empennage airloads.

The prediction of these aerodynamic forces requires suitable analysis techniques for the description of the nonuniform flow environment in which the empennage operates. The technique used herein involves the utilization of two basic programs to study these main rotor wake/empennage interaction phenomena. A wake analysis (Ref. 7) is used to determine the main rotor wake position and the strength of the vortices that are located near the empennage surfaces, and a nonlinear lifting surface analysis is utilized to predict the aerodynamic loads on empennage surfaces in the presence of these concentrated vortices. This nonlinear analysis, called RIEVA (Rotor Induced Empennage Vibration Airloads), has been formulated to include all pertinent flow phenomena such as the suction effects of the interacting vortices, span-wise induced effects, etc. For the steady-state flow case, the basic method used has predicted accurately the pressures on a swept wing in the presence of prescribed vortices as indicated by the results shown in Fig. 1 (Ref. 2 and 3). The present effort involves the extension of this analysis to account for the unsteady main rotor wake induced effects and also the effect of shed vorticity behind the empennage surfaces. The present method is an improvement over recently developed methods (e.g., Refs. 4 and 5) for the prediction of airloads because it includes nonlinear effects due to the interacting main rotor tip vortices.

2

LIST OF SYMBOLS

A	a constant, $1/2\pi^2$.
A_{mnij}	an element of the influence matrix.
$\bar{c}$	mean chord length of lifting surface, feet.
C_L, C_M, C_R	lift, pitching moment (about quarter-chord) and rolling moment coefficients, respectively, of the lifting surface; nondimensionalized to (q * Area), (q * Area * $\bar{c}$) and (q * Area * $\bar{c}$) respectively, where $q = 1/2\rho V_o^2$.
C_{LT}, C_{MT}, C_{RT}	lift, pitching moment and rolling moment coefficients, respectively, corresponding to total loads (potential plus suction airloads).
C_p	pressure coefficient, $2(p_o - p)/\rho V_o^2$.
C_T	rotor thrust coefficient.
D	doublet strength, ft^2/sec.
N	number of the collocation points.
n	subscript indicating surface normal direction.
p_o	free stream pressure, lb/ft^2.
p_u	static pressure at a point on upper surface, lb/ft^2.
p_ℓ	static pressure at a point at lower surface, lb/ft^2.
R	rotor radius, feet.
r	radial distance from a vortex center.
r_c	viscous core radius of a vortical element.
S	lifting surface area.
u,v,w	the axial, radial and the swirl velocity components of a vortex point.
V_o	free stream velocity, ft/sec.

v_n	normal component of the velocity.
V_{imom}	uniform induced velocity of rotor (momentum), ft/sec.
w_{mn}	normal velocity component at a collocation point due to all known effects, ft/sec.
x,y,z	components of the lifting surface coordinate system.
Z_A, Z_B	the vertical distances of the two ends (A and B) of a vortex element from the surface, respectively, feet.
α_o	the angle-of-attack of lifting surface with respect to free stream.
α_{TPP}	rotor tip path plane angle-of-attack, positive aft.
β_o	blade coning angle.
γ_t	turbulent kinematic viscosity of the vortex core.
Γ	circulation, ft^2/sec.
Γ_b	rotor blade bound circulation, ft^2/sec.
ΔD	incremental doublet strength, ft^2/sec.
$\Delta \ell$	incremental lift airload, lb/ft
ΔV	tangential velocity increment due to singularity.
Δt	time increment for one computational step.
ΔC_p	equals $2(p_\ell - p_u)/\rho V_o^2$.
μ	advance ratio, $V_o/\Omega R$.
η_o	distance along the direction perpendicular to the vortex-axis direction.
ρ	free stream density, lb-sec^2/ft^4.
σ	rotor solidity.

4

ϕ disturbance potential distribution.

ϕ_ℓ potential at a point on the lower surface.

ϕ_u potential at a point at the upper surface.

ψ blade azimuthal angle.

Ω rotor rotational speed, radians/sec.

II. GENERAL FORMULATION

The basic tools utilized to determine the influence of rotor airflow
on empennage excitations are the UTRC Rotorcraft Wake Analysis (Ref. 7)
and a nonlinear lifting surface analysis for unsteady three-dimensional
flow. The wake analysis is used to determine the main rotor wake induced
effects near the empennage surfaces and to provide the positions and
strengths of the vortices located near the empennage surface. The detailed
description of the technical approach, applications, and correlation re-
sults for the Rotorcraft Wake Anlaysis are presented in Ref. 7. The paths
and spacings of the vortices which would interact with the empennage sur-
faces, that is, those trailed off near the aft ($\psi = 0°$) portion of the
rotor and near the forward ($\psi = 180°$) portion of the rotor are shown sche-
matically in Fig. 2. Once the position of the interacting wake is defined,
the problem is reduced to the prediction of aerodynamic loads on lifting
surfaces in the presence of concentrated vortices. The analytical formula-
tion of this problem is described below.

Statement of the Problem

The objective of the analysis is the prediction of the unsteady airloads
on low to moderate aspect ratio lifting surface generated by the close passage
of the concentrated rotor vortices moving with the free stream. The lifting
surface is assumed to be operating at low angles of attack, with no flow
separation and the position and the strengths of the interacting vortices
are known at all instants of time. The analysis considers the unsteady incom-
pressible flow over a swept, three-dimensional wing surface of arbitrary shape
at a given angle of attack. Lifting surface theory is used to predict, in
time domain, the wing loading distributions due to the movement of the inter-
acting vortices near the surface. The analysis includes the unsteady and
suction effects of the interacting vortices, the unsteady effects of far main
wake, and the unsteady effects of the shed vorticity behind the lifting sur-
face. The interacting (viscous line) vortices are represented by finite
segments of vortical elements during their interaction with the lifting sur-
faces.

Basic Equations

Consider the coordinate system of a wing as shown in Fig. 3. The x-y plane describes the zero mean angle-of-attack plane of the wing and the z-axis is directed away from the upper surface of the wing. In this coordinate system, the positions and the strengths of the interacting vortices are defined as a function of time. Since the wing loading varies with time due to passage of these vortices, any change in wing circulation results in shed vorticity. The boundary condition for the problem is that there is no flow normal to the boundary surface.

The flow over the lifting surface is assumed to be potential; and can be described by an unknown disturbance velocity potential ϕ (x,y,z) which varies with time and is zero at points far removed from the lifting surface. Define v_n(x,y,z) as the instantaneous total normal velocity at any point on the lifting surface due to all the effects. The various components of v_n may include the induced effects of the disturbance potential at other points on the wing, the effects of shed and trailing vorticity behind the wing, the free velocity component due to angle of attack, and the velocity induced by any other known vorticity elements such as the interacting main rotor wake. The satisfaction of flow boundary condition results in

$$\frac{\partial \phi}{\partial n} = v_n, \text{ on surface S.} \tag{1}$$

Thus, the problem becomes the determination of a disturbance potential, ϕ, as a function of time in a stepwise manner caused by an airfoil moving at a constant velocity through an unsteady fluid and shedding vorticity at the trailing edge. It can be shown that assuming inviscid, irrotational, and incompressible flow the disturbance potential ϕ satisfies the Laplace equation (Ref. 8)

$$\nabla^2 \phi = 0 \tag{2}$$

at each instant of time. Thus the specific problem is the solution of the Laplace equation for the disturbance potential, ϕ, at each instant of time such that the time varying boundary condition described by Eq. (1) is satisfied.

Solution of the Laplace Equation

It can be shown that the potential function induced by singularities such as a source, or doublet, will identically satisfy the Laplace equation and will vanish at infinity. Therefore, the solution of the Laplace equation is one of finding a singularity distribution on the surface S that satisfies the normal boundary conditions in Eq. (1). Since a source distribution alone does not produce any resultant lift, a doublet distribution is required.

If D denotes a surface doublet distribution whose axis is everywhere along the outward normal to the local surface S, the potential induced at any point P is given by

$$\phi_P = -\iint_S \frac{D}{4\pi} \frac{\hat{n} \cdot \vec{r}}{r^3} \, ds \tag{3}$$

where r is the distance vector from doublet origin on S to point P, and n is the unit vector outward normal on the elemental local surface ds, and S is the total surface on which doublets are distributed. In general, the surface S consists of the upper and lower surfaces of the lifting surface and the wake surfaces.

Substitution of Eq. (3) into Eq. (1) results in the following integral equation

$$\frac{1}{4\pi} \frac{\partial}{\partial n} \left[\iint_S D \frac{\hat{n} \cdot \vec{r}}{r^3} \, ds \right] = v_n \tag{4}$$

The integration of the above equation determines the required doublet distribution D. This is carried out numerically in the analysis.

The Boundary and the Trailing Edge Conditions

The flow tangency boundary conditions (Eq. (1)) should be satisfied on the true wetted surface of the lifting surface as has been done in Ref. 3. This results in computations of the surface pressures on the upper and lower surfaces of the airfoil separately. But for this analysis, it is adequate to compute only the pressure differences between the upper and the lower surfaces. This is sufficient since no flow-separation is expected and thickness

effects are expected to be small. As a result, the no-flow boundary conditions are satisfied only along the mean line of the airfoil, thus the thickness and the curvature effects for the computations of the airloads have been ignored. This reduces computational time required and thus makes the analysis more efficient. Therefore, in this analysis the doublet distribution on the wing represents the distribution of the potential difference between the upper and lower surfaces, or

$$D(x,y,z) = \phi_u(x,y,z) - \phi_\ell(x,y,z) \qquad (5)$$

So far, in the development of the equations, wake trailing behind the wing has not been considered. It can be shown, by using the Helmholtz vorticity theorem along the trailing edge of the wing, that the doublet strengths of the wake trailing and shed elements can be expressed in terms of the doublet strengths imparted to those elements as they leave the wing. Thus, the elements on the wake do not introduce any new unknowns. In this analysis the wing wake geometry is assumed to be planar and consisting of the trailing elements extending to infinity and a finite number of shed elements, as shown in Fig. 4.

Discussion of Numerical Method

In order to integrate Eq. (4), the surface of a wing is assumed to be divided into a finite number of quadrilateral elements, as shown in Fig. 4. The value of the doublet strength D is assumed to be constant over each surface element and that the axis of the doublet is directed along the local surface normal at each control point which is at the centroid of each element. A numerical procedure is then utilized such that Eq. (4) is satisfied at a finite number of points corresponding to the centroids of the various elements representing the wing surface.

It can be shown, by analogy with electromagnetic theory, that the flow induced by a doublet distribution of density D over a given area is the same as that due to a vortex of strength D around its boundary. Therefore, numerically the doublet distribution on the surface of the wing corresponds to a network of vortex elements as indicated in Fig. 4. The Biot-Savart law is utilized to obtain the velocity field induced by the network of vortex elements. Further discussion of this approach and specifically the discussion of the computer procedure by which this is accomplished is provided in a later section (see Section III).

Determination of Pressure Distributions

Once the doublet distribution has been obtained, Bernoulli's equation is utilized for the determination of wing pressure loading under the assumption of potential flow. The loading may be described by a pressure coefficient defined as follows

$$\Delta C_p = (p_\ell - p_u)/\frac{1}{2} \rho V_o^2 \qquad (6)$$

Considering a differential element of doublet, ΔD, which represents the elemental circulation, and the velocity, ΔV, just above and below the thin elemental sheet at the mean line (average velocity V) of length, dx, the circulation is

$$\Delta D = 2 \Delta V \, dx, \text{ or } 2\Delta V = \frac{\partial D}{\partial x} \qquad (7)$$

If pressure at a distance far from the airfoil is p_o, Bernoulli's equation between the upper and lower surfaces (Ref. 8) becomes

$$\frac{1}{2} \rho V_o^2 + p_o = \rho \frac{\partial \phi u}{\partial t} + \frac{1}{2} \rho (V + \Delta V)^2 + pu \qquad (8)$$

and

$$\frac{1}{2} \rho V_o^2 + p_o = \rho \frac{\partial \phi_\ell}{\partial t} + \frac{1}{2} \rho (V - \Delta V)^2 + p_\ell \qquad (9)$$

Combining Eqs. (5), (6), (7), (8), and (9) results in

$$\Delta C_p = \frac{2}{V_o^2} \left(V \frac{\partial D}{\partial x} + \frac{\partial D}{\partial t} \right) \qquad (10)$$

10

Modeling of Nonlinear Suction Loads

Suction lift is the component of lift which results from the low pressure region within the vortices when they are in the close proximity to a lifting surface. The close interaction of a concentrated free vortex with a lifting surface can be separated into two mechanisms; one, the influence of the vortex induced velocity field, and second, the effect of the viscous core on the near field pressure distribution of the lifting surface. The first effect can be easily accounted for by including it during the determination of the potential flow field. For example, the doublet lattice method discussed in the earlier sections adequately includes the influence of the vortex induced velocity field. The modeling of the second mechanism, the nonlinear suction lift, is of significance because available experimental measurements clearly indicate that large incremental suction peaks are generated during the close wing vortex interaction and these suction peaks cannot be adequately handled by the conventional wing theories. The following section describes the analytical formulation of the suction load model incorporated in this analysis.

In general, the relative velocity at any point on a real (viscous) vortex element moving with the free stream can be described by three components, these being the swirl component w, the radial component v, and the axial component u. For example, all three of these components exist in the core of a vortex during its formation near a blade tip (or near a leading edge of a highly swept wing). During its travel from the blade tip to empennage surface, the vortex element goes through a roll up process whereby the radial and axial components of velocity become negligible and the vortex segment can then be represented by an element of a Rankine type vortex. For a Rankine type of vortex (with circulation Γ) the tangential velocity component is that of a potential line vortex outside of the viscous core region,

$$w = \Gamma/2\pi r, \text{ for } r \geq r_c, \tag{11}$$

and the velocity component is that of a rotating rigid body inside the viscous core region

$$w = \Gamma r/2\pi r_c^2, \text{ for } r \leq r_c, \tag{12}$$

so that all of the vorticity is confined to the viscous core. If we consider a Rankine vortex moving with a velocity, V_o, in the vortex outer region, the radial pressure gradient of the vortex is solely balanced by the centrifugal force term,

$$\rho w^2/r = dp/dr \tag{13}$$

The above equation is obtained from the Navier-Stokes equations described in cylindrical coordinates where the viscous and convective terms are neglected for $r > r_c$. The integration of the above equation gives

$$p = p_\infty - \int_r^\infty \rho \Gamma^2/4\pi^2 r^3 \, dr \tag{14}$$

or

$$p_\infty - p = \rho \Gamma^2/8\pi^2 r^2 \tag{14}$$

Defining the static pressure coefficient C_p as

$$C_p = 2(p_\infty - p)/\rho V_o^2 \tag{15}$$

then for a vortex in a free stream

$$C_p = (\Gamma/2\pi r V_o)^2 \tag{16}$$

The centerline of the vortex is assumed to be a streamline. Utilizing the method of images to satisfy the condition of no flow on the flat surface, the incremental ΔC_p at any point (r) on the surface is given by

$$\Delta C_p = 2C_p$$

$$\tag{17}$$

or

$$\Delta C_p = A(\Gamma/V_o)^2/r^2$$

where

$$A = 1/2\pi^2 \tag{18}$$

12

The above relationship corresponds to a simplified wing vortex inter-action model as shown in Fig. 5. For the general case where the vortex interaction with a wing is of an arbitrary nature as shown in Fig. 6, the incremental suction leading is obtained in an approximate way as discussed below.

Defining AB, as a vortex element of projected length ξ_o with a constant circulation Γ lying over a wing (see Fig. 6). Its distance from the wing (Z) varies linearly from point A to point B and can be expressed as

$$Z = Z_A + (Z_B - Z_A)(\xi/\xi_o) \tag{19}$$

The variation of suction loading in the η direction is such that the larger the distance Z, the more spread out the loading in the η-direction. In other words, the distance η_0 at which this loading goes to zero in the η-direction can be described by the approximate relationship

$$\eta_o = mZ \tag{20}$$

The value of m varies between 1 and 2. The variation of suction load ΔC_{pv} along segment AB can be written as

$$\Delta C_{pv} = K/(\eta^2 + Z^2) \tag{21}$$

where

$$K = A(\Gamma/V_o)^2 \tag{22}$$

The integrated load ($\Delta \ell$) on the wing due to segment AB is given by

$$\Delta \ell = \int_o^{\xi_o} \left[\int_{-\eta_o}^{\eta_o} \Delta C_{pv}\, d\eta \right] d\xi \tag{23}$$

Evaluation of Eq. (23) results in

$$\Delta \ell = K(2 \tan^{-1} m)\, \xi_o\, \ell n\, |Z_B/Z_A|/(Z_B - Z_A) \text{ if } Z_B \neq Z_A \tag{24}$$

13

and

$$\Delta \ell = K(2 \tan^{-1} m) \xi_o / Z_A \text{ if } Z_B = Z_A \qquad (25)$$

Similarly, the evaluation of the center of pressure of this load $\Delta \ell$ (denoted by point P in Fig. 6) is given by

$$\delta = \xi_o \left[1/(\ln |Z_B/Z_A|) - Z_A/(Z_B - Z_A) \text{ if } Z_B \neq Z_A \right] , \qquad (26)$$

where

$$\delta = \xi_o/2 \text{ if } Z_B = Z_A \qquad (27)$$

Equations (24) through (27) are used in this analysis to compute the suction loads. The value of constants A (Eq. (17)) and m (Eq. (20)) can be varied through input. Also, the values of Z_A or Z_B are always assumed to be greater than the viscous core radius of the vortex element AB.

III. DESCRIPTION OF COMPUTER PROGRAM

The analysis described in Section II has been incorporated into the computer program RIEVA (Rotor Induced Empennage Vibration Airloads). The flow chart of the key computational steps is shown in Fig. 7. The basic assumptions of the nonlinear lifting surface theory previously described are inherent in the program.

(a) It is assumed that the strength and position of the interacting vortex elements are known at all instants. In general, the circulation and the coordinates of the interacting vortical elements are input to the program. The program does have a capability, however, to compute internally the coordinates of interacting wake elements corresponding to a classical undistorted rotor wake. The equations for the description of a classical wake are given in APPENDIX A.

(b) The distortions of the interacting vortex elements due to loading on empennage surfaces are not included.

(c) The wake behind the stabilizer/fin trailing edges is assumed to consist of semi-infinite trailing elements and finite shed elements, all lying in the plane of the corresponding lifting surface (see Fig. 4). No roll up effects or distortions of this wake are included.

Numerical Method of Solution

The numerical procedure involved in applying the lifting surface method consists of dividing the surface into a number of appropriately shaped boxes. The number of these boxes is arbitrary and it is controlled through input. The magnitude of the doublet strength D over each box is assumed to be uniform. The total velocity induced perpendicular to the surface at a collocation point (centroid of the box) consists of that due to the vorticity of all other boxes on the surface, the effects of the concentrated interacting vortices, the velocity induced by the far rotor wake and that due to all the trailing and shed vorticity elements starting at the trailing edge of the lifting surface. When the flow tangency requirements on the surface are satisfied at each time step, the problem of calculating the doublet strengths is reduced to one of solving N linear algebraic equations, where N is the number of boxes on the lifting surface. Specifically, if A_{mnij} is the aerodynamic influence coefficient at the centroid of the box mn due to the effect of box ij and w_{mn} is the normal component of the velocity at collocation

15

point mn due to all known vorticity elements and due to angle of attack, the satisfaction of the boundary conditions results in the following relationship

$$\sum_i \sum_j A_{mnij} D_{ij} = w_{mn} \qquad (28)$$

Since the coordinate system chosen in this analysis is fixed to the wing at all times, the influence coefficients matrix A_{mnij} is computed only once and stored for use at subsequent steps.

Discussion of Options

One of the essential features of the RIEVA analysis is that the total main rotor wake has been split into two parts for the computations of induced velocities at the collocation points. One is the interacting elements represented by a small number of concentrated vortices which come very close to empennage surfaces causing high harmonic induced effects. The other is the induced velocities due to the rest of the wake (far wake) varying at a relatively low magnitude. As a result, far wake induced velocities are computed at relatively large intervals of time and their magnitude at intermediate intervals is calculated by interpolation. As mentioned earlier, this procedure results in savings of computational time without the elimination of high frequency effects. Some additional advantages are discussed below.

As indicated by the Biot-Savart law, the magnitudes of the high frequency airloads induced on the empennage surface depend upon the relative distance between the surface and the interacting vortex elements (besides the circulations of the vortex elements). For a helicopter rotor in forward flight, only the undistorted wake can be described by analytical means. It is very difficult to compute accurately the distortions of the wake elements while they move from rotor blade to the empennage surface. In fact, some of these interacting elements go through distortions of very large magnitude due to encounters with rotor hub, fuselage, etc. Therefore, the positions of the interacting vortices with respect to the empennage surfaces can only be approximated. In the RIEVA analysis, since the interacting rotor wake is represented by a limited number of vortices (normally blade tip vortices), it becomes relatively easy to modify their geometry and thus compute the airloads corresponding to the modified wake geometry. As a result, once the approximate position of the wake is defined, the interactions could be realistically assumed to occur anywhere within the envelope described by varying the distance between the empennage surfaces and the vortices. The analysis

16

is flexible enough to consider many types of interactions. Specifically, the interacting vortices can be arbitrarily moved closer to the empennage surface to determine the magnitude of the critical airloads corresponding to the extreme cases of wake distortions. Thus, wake distortion effects can be accounted for indirectly and thereby the analytical computations of the distorted rotor wake geometry are avoided.

The various options available in the RIEVA analysis for describing the interacting wake coordinates and the rotor induced velocities are described below.

For interacting wake geometry description, the user has the option to input the coordinates of interacting wake elements at each instant of time. This is particularly useful for those cases where the distorted wake geometry is known. Alternately, the user can utilize the wake coordinates computed internally by the RIEVA analysis. For a given flight condition and rotor parameters, the program computes the wake coordinates corresponding to the classical undistorted skewed helical wake.

Also, for the inclusion of far wake effects, there are two options available. For one option the user can compute the induced velocities at empennage points due to all or part of the rotor wake by utilizing a Rotorcraft Wake Analysis (Ref. 7) and input these velocities to the RIEVA analysis. Alternatively it may be assumed that the far wake induces a uniform velocity at the empennage points and its magnitude is described through input. This approximation may be valid for some high speed flight conditions. The coupling of program RIEVA with the Rotorcraft Wake Analysis is further discussed in the following section.

Coupling With Program F389

As indicated in the flow chart (Fig. 7), the Rotorcraft Wake Analysis (Program F389, Ref. 7) may be utilized to obtain some of the inputs required for the execution of program RIEVA. These inputs may be divided into three convenient groups as described below.

1. The circulations of the interacting vortex elements can be determined by utilizing the Program F389. For a given rotor configuration, with known control inputs, Program F389 computes the radial and azimuthal distribution of the blade circulation, $\Gamma_b(r,\psi)$. Once the distribution, $\Gamma_b(r,\psi)$, is prescribed, the circulations of the interacting vortices can be very easily estimated by using a simple roll up theory. Normally these interacting vortices will consist of only the blade tip vortices that are trailed off the fore and the aft portions of the rotor disk.

17

2. The induced velocities at the empennage collocation points due to main rotor wake may be computed by utilizing the Program F389. Normally, these induced velocities are computed at coarse intervals of time and the effects of the interacting elements (elements in group 1. above) are excluded from these computations (this is done to avoid redundancy).

3. If desired, the coordinates of the interacting elements can also be obtained from the output of the computer program F389.

Interacting Vortex Geometry Modifications

This section describes the procedures utilized by the RIEVA program to automatically modify the geometry of the interacting wake elements in case these elements intersect the empennage surfaces. This is carried out in a very approximate manner. The use of this procedure is optional and it is specified through input to the program.

Figure 8 illustrates the modifications involved. The modifications are confined to junction points (where the various elements of vortex meet). The junction point nearest to the wing surface (only if the vortex element is cut) is modified, as shown in Fig. 8. The junction point is always kept at least one core radius (viscous core radius r_c) away from the surface. Also the modified junction points at locations above the wing are not allowed to penetrate the surface at subsequent time steps, but instead they are allowed to slide over the wing surface (or even some distance beyond the trailing edge, this distance being specified through input).

The modifications described above involve the changing of only the Z-coordinate of the affected vortex elements. No attempt is made to determine the vortex displacements from their original position due to the wing vorticity field.

Future Capabilities

Some of the improvements that may be carried out in the future to enhance the capabilities of the RIEVA program are discussed in the following section.

1. At present a considerable amount of user judgement is required to divide the main rotor wake into two parts; one, the interacting elements and two, the far wake elements. A procedure should be developed and then incorporated in the RIEVA analysis whereby this splitting of wake is carried out automatically within the program.

18

2. The nature of the interaction between the main rotor vortices and the vertical tail is such that significantly large streamline velocities may be induced on the tail surface by these interacting vortices. This span-wise variation of the streamwise velocity results in a significant amount of vibratory airloads being generated by the vertical tail. At present, RIEVA analysis does not account for these effects.

3. The coding and the dimensions of the RIEVA program should be modified so that the airloads acting on the vertical fin and the horizontal stabilizer can be computed simultaneously.

4. Flow separation effects should be included in the RIEVA analysis. Normally, when a vortex is close to the surface, flow separation occurs on the upwash side of the vortex.

IV. PROGRAM RIEVA DOCUMENTATION

The computer program for the determination of rotor induced empennage vibration airloads (RIEVA) incorporates a number of key options. The inclusion of these options results in computer efficiency and provides flexibility on the type and source of the interacting wake elements.

The program documentation includes

(i)   a brief description of program subroutines,
(ii) a detailed description of input data,
(iii) a brief description of program output.

Subroutine Descriptions

A brief description of each of the subroutines is given below in alphabetical order.

Subroutine COLLOC

This subroutine computes the aerodynamic influence coefficient matrix A_{mnij} at the first time step and stores it on unit 10 for use at subsequent time steps. It also computes the coordinates of the collocation points and prints out the coordinates, if requested.

Subroutine DMAT

This subroutine computes the solution of a set of simultaneous algebraic equations of order N.

Subroutine GETVIS

This subroutine interpolates input induced velocity components corresponding to the far rotor wake at the intermediate time steps.

Subroutine HARMPM

This subroutine computes the harmonic coefficients of the wing aerodynamics loads.

Subroutine LOADER

This subroutine reads in the loader input data.

Subroutine LOADS

This subroutine computes and then prints out the wing aerodynamic loading distribution ΔC_R at each time step. Also, the total wing aerodynamic loads are computed and printed out.

Subroutine MAIN

This is the main routine. It calls subroutines LOADER, PRNT, WLINPT, COLLOC, VRTXG, SLOAD, GETVIS, VELKNW, SOLVEG, LOADS and HARMPM and prints out the harmonics of the wing airloads. It also prints out the instantaneous geometry of the interacting vortices.

Subroutine OUTPUT

This is a general subroutine which prints out the chordwise and spanwise distribution of the various quantities (e.g., doublet distribution D, pressure distribution Δc_p, etc.)

Subroutine PRNT

This subroutine prints out all the input loader data.

Subroutine SLOAD

This subroutine computes the nonlinear suction airloads, when requested.

Subroutine SOLVEG

This subroutine sets up the simultaneous set of algebraic equations to be solved at each time step, and also, outputs the computed doublet distribution.

Subroutine UVW

This subroutine computes the induced velocities due to a vortical element.

Subroutine VELKNW

This subroutine computes the induced velocities at the collocation points due to the interacting vortices and also due to the wing wake trailing and shed elements.

Subroutine VRTXG

This subroutine computes the coordinates of the interacting main rotor vortices corresponding to a classical undistorted wake model.

Subroutine WLINPT

This subroutine reads in the main rotor far wake induced velocities and converts them to the wing coordinate system. It also prints out the distribution of the normal component of these far wake induced velocities corresponding to each time step.

Input Description

The required input to the program consists of the following major punched card data blocks, in order of loading:

I. Wing (Empennage), Vortex Geometry and other Solution Control Data (in Loader Format)

II. Induced Velocity Data due to Far Main Rotor Wake (Optional)

III. Interacting Vortex Geometry Data (Optional)

Details for preparing these blocks of data are given in the following sections.

I. Empennage, Vortex Geometry and Other Solution Control Data

This block of data is split into the following three groups.

(a) Solution Control Parameters
(b) Empennage
(c) Vortex Geometry Parameters (Optional)

The group (a) contains the data that determines which of the various options are to be exercised. The data in this group are loaded in an array (SCP). The group (b) contains data that describes the empennage surface geometry and the free stream parameters. This group of data is stored in WCP array. The group (c) contains the rotor data needed to describe the interacting main rotor wake geometry based on a classical undistorted model of the rotor wake. This group of data is stored in array VCP. If internal computation of the interacting wake geometry is not required, this group of data may be omitted.

22

The order in which the groups of data are loaded is arbitrary. The format for these data is as follows:

A N L DATA(L) DATA(L+1) . . . . DATA(L+4)   (A1, I1, I4, 5F12.0)

where A, in Column 1, represents the letter S, W or V corresponding to arrays SCP, WCP or VCP. N is the number of data items to be input on the card Column 2; N must not exceed 5. L is the location or identifying number of the first data item on the card Columns 3-6, right adjusted. DATA(L+j) represents the various data items on the card, Columns 7-18, 19-30, 31-42, 43-54, and 55-66, in floating point format. The locations for the various data are listed below along with definitions and other pertinent comments. Note that some locations are intentionally left blank.

(a) SCP Array Data

Location	Item	Description
1	N_W	The number of lifting surfaces. For horizontal stabilizer $N_W=2.$, one for each semi-span. For vertical tail, $N_W=1$. At present both stabilizer and fin cannot be modeled simultaneously.
2	MYES	MYES-1., doublet lattice method is applied. MYES=0., no doublet solution required; this option is used if only nonlinear suction loads are desired.
3	NSHED	Specifies the number of shed elements to be included in the wing wake. Range is 0. to 5. (see Fig. 4).
4	MSYM	Normally MSYM=0. When MSYM=1., the program assumes symmetrical loading on both the right and left hand sides of the stabilizer.
5	NVORT	Specifies the number of interacting vortices. Range is 0. to 8.
6	IVGEOM	Option for the description of the interacting wake elements. IVGEOM=0, rotor wake data specified via loader inputs in VCP array (group c). IVEGOM=1, interacting wake data input at each time step. This is described separately (data block II, Page 29).

Location	Item	Description
7	NFARF	Option for including the far wake induced velocity effects. If NFARF=1, this component of the induced velocities is to be input as described separately (data block II). If NFARF=0, no data are read in. If desired, under this option (NRARF=0), these effects may be accounted via input in location 19 of SCP array.
8	MODVG	Option to modify the interacting vortex geometry if the vortex gets cut by the empennage surface (see Section II, Page 13). For MODVG=0, no modifications are carried out.
9	EXT	If MODVG=1 (previous location), the area of the wing surface over which the modifications are to be carried out is extended via input in this location, i.e., the modifications of the vortex are carried out even beyond the wing surface. EXT is nondimensionalized with respect to the mean chord length of the wing.
10	INSUC	Option to include the computations of nonlinear suction loads. INSUC=1, loads are computed. INSUC=0, no loads are computed.
11	NT	Specifies the total number of time steps for which computations are to be carried out.
12	ΔT_2	Specifies time increment per step, secs.
13	MHDO	Option to perform an harmonic analysis of the computed air loads over one period. For MHDO=1, Yes and for MHDO=0, No. The number of points per period is specified in location 15.

Location	Item	Description
14	NH	If MHDO=1 (location 13), the input specifies the number of harmonics desired.
15	NT2	Specifies the number of steps per period.
16	A	The constant A in the suction airload model (Equation 18) if different from $1/2\pi^2$ (default value).
17	T_n	The parameter $(2 \tan^{-1} m)$ in the suction airload model (Equation 25) if different from 2.21429 (default value).
18	e_{fm}	Factor to modify the first shed element from the TE. Included for possible future use (Reference 10). A nonzero positive value of e_{fm} (0. to 1.) models the first shed element closer to the TE by the factor e_{fm}.
19	F_v	If the effects of the far rotor wake are represented by a constant uniform induced velocity over the wing, its magnitude is input here. It is non-dimensional with respect to V_{imom} (positive downwash) which should be input in location 3 of VCP array.
20	–	Not used.
21	LPCOLL	Print option for coordinates of the collocation points over wing. LPCOLL=1, Yes. LPCOLL=0, No.
22	LPVRTX	Option to print vortex geometry coordinates at each time step. LPVRTX=1, Yes. LPVRTX=0, No.
23	LPINDV	Option to print the total (near plus far wake) induced velocity distribution at each time step. LPINDV=1, Yes. LPINDV=0, No.

25

Location	Item	Description
24	LPDBLT	Option to print the doublet distribution at each time step. LPDBLT=1, Yes. LPDBLT=0, No.
25	LPPRCP	Option to print the airload distribution ΔC_p at each time step. LPPRCP=1, Yes. LPPRCP=0, No.
26	LPFARW	Option to print the inputted (data block II) far-wake V_i distribution. LPFARW=1, Yes. LPFARW=0, No.
27	LPSUCD	Option to print the computed nonlinear suction airloads. LPSUCD=1, Yes. LPSUCD=0, No.
28	IDEBUG	Option to print debug parameters. Always input IDEBUG=0.

(b) WCP Array Data

Location	Item	Description
1-2	X_1, Y_1	X and Y coordinates of corner 1 of the first surface in the wing coordinate system illustrated by Figure 4 (feet).
3-4	X_2, Y_2	X and Y coordinates of corner 2 (feet).
5-6	X_3, Y_3	X and Y coordinates of corner 3 (feet).
7-8	X_4, Y_4	X and Y coordinates of corner 4 (feet).
9	N_c	Number of chordwise stations for the lattice of the first wing.
10	N_s	Number of spanwise stations for the lattice of the first wing.
11-20	(")	Specifies the parameters for the second wing in the same order as for the first wing (in locations 1 through 10).

Location	Item	Description
21	V_o	Magnitude of free stream velocity, ft/sec.
22	α_o	The angle of attack of wing, deg.
23	$\bar{C}$	Mean reference chord, ft.
24	ρ	Density of free stream medium, $\text{lb-sec}^2/\text{ft}^4$.

(c) VCP Array Data

Input of this data is optional. Input only if the value in location 6 of SCP array is 0, and the value in location 5 of SCP array is greater than 0.

Location	Item	Description
1	ΩR	Blade tip speed, ft/sec.
2	R	Blade radius, ft.
3	V_{imom}	Uniform momentum induced velocity, ft/sec. (positive for inflow or positive thrust)
4	α_{TPP}	Tip path plane angle of attack, deg. (positive aft).
5	β_o	Rotor cone angle, deg.
6-8	X_h, Y_h, Z_h	X, Y and Z coordinates of rotor hub, specified in the wing coordinate system, ft. (see Figure 3).
9	γ_c	Eddy viscosity of the vortex core, ft^2/sec. Required to compute the increase in core radius with time (see Equation B-1 , in Appendix B).
10	IFB	Option for the inclusion of blade bound circulation effects by modelling it as one of the elements interacting with empennage. If the blade passes very close to the empennage, IFB should be input as 1.

Location	Item	Description
11	f_b	Nondimensional factor (between 0. to 1.) to multiply the maximum blade circulation in order to get effective circulation.
12	N_b	Number of rotor blades.
13	L_R	This is the input required to make the time reference of data block II compatible with the time reference of the interacting wake geometry. L_R is the reference step number in data block II that corresponds to starting time (t=0) of wake geometry computations.
14-20	-	Not used.
21	ϕ_1	Azimuthal location at which the first point of the vortex is trailed, deg. (see Equation A-4).
22	ψ_a	Age of the first point of the vortex, deg. (see Equation A-5).
23	$\Delta\psi$	Azimuthal increment, deg. (see Equation A-4).
24	$\Delta\psi_{ru}$	Time for the vortex to roll up to the initial core radius r_{co} specified in location 25, deg.
25	r_{co}	Initial core radius of the vortex, ft.
26	r_b	Radial location on blade from which the vortex is trailed (nondimensional). $r_b=1$ corresponds to tip vortex (see Equations A-1, A-2).
27	$\Delta\psi_2$	Azimuthal increment used in the computation of the far wake effects, deg. Required for the aft forming vortex only.
28-29	-	Not used.

Location	Item	Description
30	N_v	Number of segments representing the vortex. Maximum of 9.
31-39	Γ_v	Circulations of segments, ft^2/sec.
40	-	Not used.
41-59	(")	Corresponding data for the second vortex similar to those for the first vortex in locations 21-39.
60-179	(")	Similar data for the remaining six vortices.

II. Induced Velocity Data (Optional)

This block of data is required only if the value of location 7 of the SCP array (see data group a) is 1.0. F389 (Ref. 7) (see Section III, Page 17) generates this data in a format which is compatible with the input requirements of RIEVA program. This block of data consists of three components of the instantaneous induced velocity at each of the collocation points. These induced velocities are described in the rotor tip path plane coordinate system (see Appendix A). Also, these induced velocities are described for various time steps; the total time covered being exactly the time for one blade passage. The first card of this data block contains three quantities; LS, ΔT, and NTOT is the format (I2, F20.0, I5). LS is the total number of time steps, ΔT, is the time in seconds corresponding to each step and NTOT is the total number of collocation points. The total number of quantities (N_d) contained in the data (following the first card) is

$$N_d = 3 \times LS \times NTOT$$

where 3 represents the three components of induced velocity.

These N_d numbers are input in order with six quantities per data card, in the format (6F12.0).

III. Interacting Vortex Geometry Data (Optional)

This block of data is required only if the value of location 6 of SCP array (see data group a) is 1.0. This input data block describes the instantaneous locations and strengths of all the interacting vortex elements. This option may be utilized if the interaction between the empennage and the vortices is of non-periodic (transient) nature. Also, if the main rotor wake distortions are known, the wake data for these distorted elements may be input via this block.

For each of the vortices, the following quantities are input.

Card #	Quantity or Quantities	Format
1	N_V (Number of vortex points)	(I5)
2	x,y,z,R,Gv (for first point)	(5F10.6)
	where: x,y,z are the coordinates in the wing coordinate system, R,Gv are the viscous core radius and the circulation respectively.	
3	x,y,z,R,Gv (for second point)	(5F10.6)
N_V+1	x,y,z,R,Gv (for N_Vth point)	(5F10.6)

The above information is input for all the NVORT (see location 5 of SCP array) vortices.

The above information is repeated for each time step until data for all time steps has been input.

Output Description

A brief description of the printed output generated by the RIEVA program is given here. The amount and the nature of the output for a particular run is controlled through the exercise of various print options specified via input in locations 21-27 of the SCP array (see Section IV, Page 25).

The RIEVA program output can be classified into the following ten major categories (in order of output).

1. Listing of Input Loader Data
2. Listing of Input Far-Wake Induced Velocities
3. Coordinates of Collocation Points
4. Instantaneous Description of Interacting Vortices
5. Instantaneous Induced Velocity Distribution
6. Instantaneous Doublet Distribution
7. Instantaneous Airload Distribution
8. Instantaneous Integrated Airloads
9. Nonlinear Suction Loads (if present)
10. Harmonics of Airloads

The categories 2., 3., 5., 6., and 7. listed above involve the chordwise and spanwise variation of the various quantities and are printed out in a similar format by the subroutine OUTPUT. Category 3. provides the coordinates of the various collocation points over all the surfaces, and the numbers in the output categories 2., 5., 6., and 7. represent the values of the various quantities at the corresponding points (listed in category 3.).

Most of the output of RIEVA analysis is self-explanatory; only a brief description of each category is provided. No samples of the output are included here. Also it should be noted that categories 4. through 8. are output at each time step.

1. Listing of Input Loader Data

This is output by Subroutine PRNT, which lists the values of all the input loader data (discussed in Section IV. under Input Description: Data Block I.).

2. Listing of Input Far-Wake Induced Velocities

This is output by Subroutine WLINPT, which lists the input induced velocities at the empennage points. First the total number of time intervals and the time (in seconds) corresponding to each interval are printed out.

3. Coordinates of Collocation Points

This output by Subroutine COLLOC, which lists first the x-coordinate of the control points and then the y-coordinate of the control points in the wing coordinate system. Before these collocation points are listed, the coordinates of the corners of the various control surfaces modeled (along with some flight parameters) are given first.

4. Instantaneous Vortex Geometry

This is output from program MAIN and consists of the description of position and strength of the various elements of the interacting vortices. First the step number and the time (in seconds) corresponding to that step are printed out. Next, for each junction point of the interacting vortices, x, y and z coordinates (in wing coordinate system) are listed. Also the circulation (ft**2/sec.) and the viscous core radius (feet) of each of the elements are listed. Finally a quantity ZMOD is listed. If

the value of ZMOD is 1.0, it indicates that the z-coordinate of the junction corresponding to that point has been altered according to the procedure given in Section III, Page 18).

5. Induced Velocity Distribution

This is output by Subroutine SOLVEG, which describes the instantaneous total induced velocity (due to far wake plus interacting wake) distribution (positive downwash).

6. Doublet Distribution (listed as 'SOLUTION GAMMAS')

This is output by Subroutine SOLVEG, which lists the computed doublet distribution over the control surfaces. A positive value corresponds to a clockwise direction of the vortical elements around the box (see Fig. 4.).

7. Attached Flow Airload Distribution

This is output by Subroutine LOADS, which describes the unsteady ΔC_p ($\Delta C_p = C_{p\ell}' - C_{pu}$) or airload distribution over the surface.

8. Integrated Airloads

This is output by Subroutine LOADS. At the end of the output of each step, the integrated loads for the total surface are listed. Both the nondimensional coefficients C_L, C_M, and C_R, and the dimensional loads L (lbs), PM (lb.-ft.) and RM (lb.-ft.) are printed out.

9. Nonlinear Suction Loads (if present)

This is output from program MAIN and consists of the integrated suction loads (ΔC_{LV}, ΔC_{LM} and ΔC_{RM}) for all the time steps over one blade passage. These are listed under the heading "Suction Loads Variation".

10. Harmonics of Airloads

This is printed out from program MAIN. The airload (C_L, C_M or C_R) variation over one blade passage is converted into mN_b per rev (N_b = number of blades, m=1,2,3,etc) harmonic airloads. For example total C_L is expressed as

$$C_L = a_o + \sum_{m=1}^{M} a_m \cos (mN_b \psi) + b_m \sin (mN_b \psi)$$

or

$$C_L = a_o + \sum_{m=1}^{M} r_m \sin (mN_b \psi + \phi_m)$$

For each load the quantities a_o, $[a_m$, b_m, r_m, ϕ_m (for m=1, ...M)] are printed out. Maximum value of M is 4. The various loads that are harmonically analyzed are listed below in the order of their print out:

1. C_L, C_M and C_R for control surface 1.

2. C_L, C_M and C_R for control surface 2.

3. C_L, C_M and C_R for total (1+2) surface

4. ΔC_{LV}, ΔC_{MV} and ΔC_{RV} representing the incremental airloads due to nonlinear suction.

V. RESULTS AND DISCUSSION

This section presents and analyzes the results obtained from the RIEVA (Rotor Induced Empennage Vibration Airloads) program for some realistic check cases.

The basic check case chosen involved the computation of the unsteady airloads acting on the Black Hawk horizontal stabilizer surface for a high speed forward flight condition of 172 knots. Calculation of the strength of the interacting vortex elements and the induced velocities at the stabilizer points due to the rotor far wake were necessary before RIEVA could be executed. An undistorted classical wake model and trimmed forward flight were assumed for the calculations. The various flight and control parameters for this case are listed in Table I. The variation of the maximum blade circulation (Γ_{bm}) with blade azimuth position (ψ) is shown in Fig. 9. The total rotor wake has been split into two parts, one, the interacting wake elements and two, the far wake as shown in Fig. 10. The interacting wake elements comprised the segments of the blade tip vortices trailed off the forward and aft portions of the rotor (30 deg. on each side of the centerline or the x-axis). The circulations of these tip vortex elements were the values of Γ_{bm} in Fig. 9.

The far wake induced velocities at the stabilizer points were computed (using Rotorcraft Wake Analysis F389) at time intervals corresponding to $\Delta\psi$ ($\Omega * \Delta t$) of 15 degrees. For one representative point on the stabilizer surface (at quarter chord point on the centerline), the variation of the far wake induced velocity with time is shown in Fig. 11. Also shown in Fig. 11 is the variation of the total induced velocity (due to interacting wake plus far wake) with time. Examination of Fig. 11 reveals that most of the high frequency variation of the total induced velocity is caused by the interacting wake elements. This result substantiates the assumption that the computations of the far-wake induced velocities are only necessary at coarse intervals of time.

RIEVA was used to calculate the instantaneous positions of the interacting vortex elements at fine intervals of time. For the basic case the total time corresponding to one blade passage (T = 0.05814 seconds) was divided into 12 equal steps and the computations were carried out every .004845 seconds. At three such instants (steps 1, 7, and 12) the paths and spacings of the interacting rotor blade tip vortices with respect to the horizontal stabilizer are described in Figs. 12, 13, and 14, respectively. In these figures, the vortices numbered 1, 2, and 3 are those trailed off

34

the forward portion of the rotor (ψ = 210 to 150 degrees) while the vortices numbered 4 and 5 are those trailed off the aft (ψ = 30 degrees to -30 degrees) portion of the rotor. The integrated unsteady airloads of the stabilizer (at zero angle of attack) are shown in Fig. 15 as a function of time ($\psi=\Omega t$). In this figure C_{LT} is the lift coefficient (normalized to $.5\rho V_o^2$ x wing area). C_{MT} is the pitching moment coefficient about the quarter chord (positive up), and C_{RT} is the rolling moment coefficient about the stabilizer centerline (positive for right side going down); both of these moment co-efficients are normalized ($.5\rho V_o^2$ x wing area x mean chord). As expected, the airloads C_{LT}, C_{MT} and C_{RT} are periodic with each blade passage (or every 90 degrees for four-bladed rotor). The computations have to be carried out for more than one blade passage (as shown in Fig. 15), since the strengths of the shed elements were not known at the start of the computa-tions. Once the shed vorticity develops (after 5 to 6 steps), the results indicate excellent periodicity with each blade passage (as indicated by the results shown in Fig. 15). The airloads' variation over one period was converted into the 4m per rev (m = 1, 2, 3) harmonic airloads and result in the following vibratory airloads on the stabilizer:

$$C_{LT} = -0.184 + 0.127 \sin (4\psi - 90°)$$
$$+ 0.068 \sin (8\psi + 168°)$$
$$+ 0.032 \sin (12\psi - 36°)$$

$$C_{MT} = -0.0032 + 0.0187 \sin (4\psi + 129°)$$
$$+ 0.0161 \sin (8\psi - 8.3°)$$
$$+ 0.0112 \sin (12\psi + 144°)$$

$$C_{RT} = -0.0058 + 0.0773 \sin (4\psi + 195°)$$
$$+ 0.0750 \sin (8\psi + 98°)$$
$$+ 0.0400 \sin (12\psi - 31°)$$

The airloads described above are the total loads being applied to the stabilizer of the helicopter and these can be used as input to the coupled rotor/airframe (Ref. 6) vibration analysis. The computer program RIEVA also provides a detailed description of these airloads (chordwise and span-wise variation of ΔC_P). These airloads may be utilized to study the aero-elastic vibrations of the empennage itself. As an example, for this check case some calculated airload distributions are shown in Figs. 16 and 17 (for three spanwise stations; at 6% and 56% stations on the right stabilizer and at 56% station on the left stabilizer). Figure 16 describes these airload distributions at the time step No. 1, the instantaneous vortex geometry for which is illustrated in Fig. 12. The chordwise variation of the airload at this instant resembles the conventional airload distribution observed on

an airfoil at a negative angle of attack. But when a concentrated vortex is directly above the stabilizer (such as vortex number 2 in Fig. 13), these chordwise airload distributions look totally different. This is clearly indicated by the distribution of the airloads described in Fig. 17, which correspond to the time for which the instantaneous vortex geometry is described in Fig. 13. These deviations are obviously due to the unsteady effects caused by the presence of the moving vortex.

As indicated by Figs. 12, 13 and 14, the closest distance between the stabilizer surface and the interacting vortices is approximately 1.5 feet. If this distance were smaller (say less than three times the viscous core radius of the vortex), either due to wake distortion or due to change in tip path plane angle of attack, an additional component of the airloads results. As discussed before, this component of the air-loads is due to the nonlinear suction effects that occur when the vortex passes very close to a surface.

An additional check case was run to verify the modeling of the non-linear suction airloads in the RIEVA analysis. This case corresponds to the same flight conditions as described earlier (see Table I) except that the tip path plane angle was arbitrarily increased to -14.42 degrees. This was done to let the vortices off the front portion of the rotor pass very close (within 2 inches) to the horizontal stabilizer surface (see vortex #2 in Fig. 18). As a result of close stabilizer-vortex interaction, significant nonlinear suction airloads result and as shown in Fig. 19 for one blade passage. These incremental suction airloads (ΔC_{LV}, ΔC_{MV}, ΔC_{RV}) have to be added appropriately to the potential flow loads (C_L, C_M, and C_R shown in Fig. 20) in order to determine the total loads C_{LT}, C_{MT} and C_{RT}. These total loads are shown in Fig. 21 for one blade passage. It should be remembered that the loads described in Fig. 21 have been computed under the assumption that no flow separation of any kind occurs. Normally flow separation occurs on the upwash side of the vortex during the close airfoil-vortex interaction. At present the RIEVA analysis does not account for these flow separation effects.

VI. CONCLUSIONS AND RECOMMENDATIONS

A computer program (RIEVA) has been developed that predicts the unsteady aerodynamic forces that are imposed on the empennage surface due to its interactions with the main rotor wake. The program was exercised to determine the vibration airloads acting on the Black Hawk horizontal stabilizer for a high speed (μ = 0.4) forward flight condition. The following are specific conclusions obtained from analysis of the Black Hawk simulation.

1. The results demonstrate that it is possible to compute the high frequency empennage vibration airloads (up to 16 revolution) efficiently (reasonable amount of computer time) by utilizing this analysis. This check case required only 4 to 5 minutes computer time on an IBM 370 system.

2. No numerical problems were encountered, and the airload harmonics converged quickly.

The following future activities are recommended:
*
1. A correlation study should be carried out to compare the RIEVA predicted empennage airloads with test data.

2. The RIEVA analysis should be extended to account for the spanwise variation in streamwise velocity (nonuniform free stream velocity). The inclusion of this feature will result in the analytically correct computation of the vertical tail airloads and provide the capability of studying the blade finite tip-vortex interaction problem.

*
The draft copy of the present report was prepared in 1981. Since then a limited correlation study has been carried out wherein the RIEVA predicted stabilizer airloads have been compared with the CH-53A flight test data. The results indicate a reasonably good correlation between analytical predictions and the flight test data. These results are presented in the following Reference:

Gangwani S. T.: Determination of Rotor Wake Induced Empennage Airloads. Presented at the American Helicopter Society National Specialists' Meeting on Helicopter Vibration, Hartford, CT., November 2-4, 1981.

VII. REFERENCES

1. Sheriden P. F. and R. P. Smith: Interactional Aerodynamics - A New Challenge to Helicopter Technology. Presented at the 35th Annual National Forum of the American Helicopter Society, Washington, D. C., May 1979, Preprint No. 79-59.

2. White, R. P., Jr., S. T. Gangwani and J. C. Balcerak: A Theoretical and Experimental Investigation of Vortex Flow Control for High Lift Generation. Report ONR-CR212-223-3, prepared by RASA, a Division of Systems Research Laboratories, Inc., Newport News, Virginia, December 1976.

3. White R. P., Jr., S. T. Gangwani and D. S. Janakiram: A Theoretical and Experimental Investigation of Vortex Flow Control for High Lift Generation. Report ONR-CR212-223-4, prepared by RASA, a Division of Systems Research Laboratories, Inc., Newport News, Virginia, December 1977.

4. Jordan, P. F.: Reliable Lifting Surface Solutions for Unsteady Flow. AIAA 16th Aerospace Sciences Meeting, Huntsville, Alabama, January 1978.

5. Geissler, W.: Nonlinear Unsteady Potential Flow Calculations for Three-Dimensional Oscillating Wings. AIAA Journal, Vol. 16, No. 11, pp. 168-174, September 1978.

6. Sopher R., R. E. Studwell, S. Cassarino and S. B. R. Kottapalli: Coupled Rotor/Airframe Vibration Analysis, NASA CR-3582 Contract NAS1-16058, June 1982.

7. Landgrebe, A. J. and T. A. Egolf: Rotorcraft Wake Analysis for the Prediction of Induced Velocities. USAAMRDL Tech. Report 75-45, Eustis Directorate, USAAMRDL, Fort Eustis, Virginia, January 1976.

8. Karamacheti, K.: Principles of Ideal-Fluid Aerodynamics. John Wiley and Sons, Inc., 1966.

9. Piaziali, R. A.: Method for the Solution of the Aeroelastic Response Problems for Rotating Wings. Journal of Sound and Vibration, Vol. 4, No. 3, pp. 445-486, November 1966.

Table I

BLACK HAWK CHECK CASE PARAMETERS

Free Stream Velocity, Knots	172.0
Advance Ratio, μ	0.39
Blade Radius, Feet	26.83
Thrust, Pounds	17,203
C_T/σ	.0902
Tip Path Plane Angle, Degree	−10.8
Cone Angle, Degree	3.66
Uniform Momentum Induced Velocity, FPS	6.67
Rotor Solidity, σ	0.0821
Number of Blades	4.0
Hub X-coordinate, Feet	28.25
Hub Y-coordinate, Feet	0.0
Hub Z-coordinate, Feet	6.25
Area of Stabilizer, Square Feet	44.45
Mean Chord of Stabilizer, Feet	3.083
Stabilizer Angle of Attack, Degree	0.000

APPENDIX A

The wake equations for a rotor in forward flight, based on the classical undistorted helical wake model, are presented below. These equations are utilized in the analysis (RIEVA) to describe the geometry of the vortices that interact with the empennage surface. The equations are described in the rotor tip path plane coordinate system. The rotor hub location is the origin, the x-axis is positive aft, the y-axis is positive to the right (ψ = 90 degrees) and z-axis is pointed up (right-handed cartesian coordinate system). The azimuth angle ψ is measured with respect to positive x-axis, rotating counterclockwise.

The coordinates of any point n on the vortex trailed from the blade radial location r_b (nondimensionalized to R) can be described as follows:

$$X_{nt} = \mu_{TPP} \psi_a + r_b \cos(\phi_n) \tag{A-1}$$

$$Y_{nt} = r_b \sin(\phi_n) \tag{A-2}$$

$$Z_{nt} = \lambda_{TPP} \psi_a \tag{A-3}$$

with

$$\phi_n = \phi_1 - (n-1) * \Delta\psi \tag{A-4}$$

$$\psi_a = \phi_b - \phi_n \tag{A-5}$$

$$\mu_{TPP} = V_o \cos(\alpha_{TPP})/\Omega R \tag{A-6}$$

$$\lambda_{TPP} = -V_{imom}/\Omega R + V_o \sin(\alpha_{TPP})/\Omega R \tag{A-7}$$

where

$\Delta\psi$ is the incremental ψ to describe various segments,

n   varies from 1 to the maximum number of points chosen,

ϕ_b describes the current position of reference blade,

ψ_a represents age of the wake point, and

V_{imom} is the uniform momentum induced velocity

APPENDIX B

The mathematical model for the determination of the viscous core radius of the blade tip vortices is described in this appendix. In the RIEVA analysis the computation of the core radii is required only when the interacting vortices come very close to the empennage surface. It is assumed that after roll up, the viscous cores can be represented by a constant turbulent eddy viscosity model. Under this assumption the core radius r_c, increases with time as given by the following relationship:

$$r_c^2 = r_{co}^2 + \beta^2 \gamma_t \ (\psi_a - \psi_{ru})/\Omega \qquad \text{(B-1)}$$

where

r_{co} = core radius at time of roll up, ψ_{ru}.

γ_t = turbulent eddy viscosity of core.

β^2 = a constant, $(0.716)^2$.

ψ_a = age of the vortex element,

Ω = rotational speed

The magnitudes of r_{co}, ψ_{ru} and γ_t have to be obtained empirically and input to the RIEVA program.
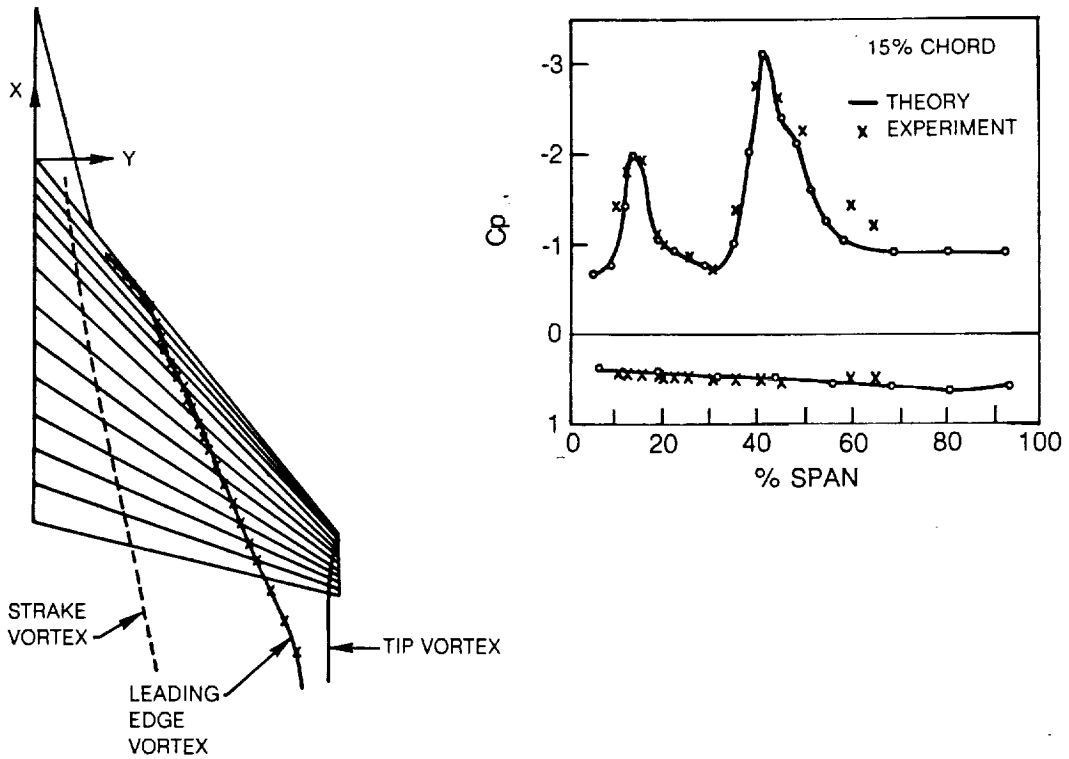
Figure 1. Wing/Vortex Geometry and Comparison of Measured and Predicted Chordwise Pressure Distribution from Reference 3
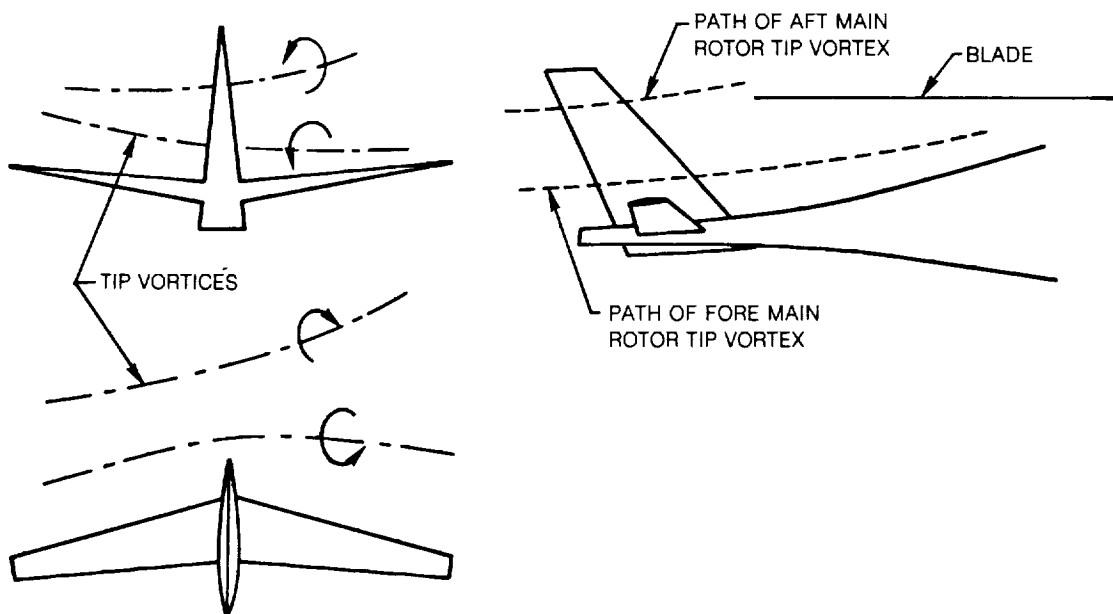
Figure 2. Schematic of Main Rotor Tip Vortex/Empennage Interaction
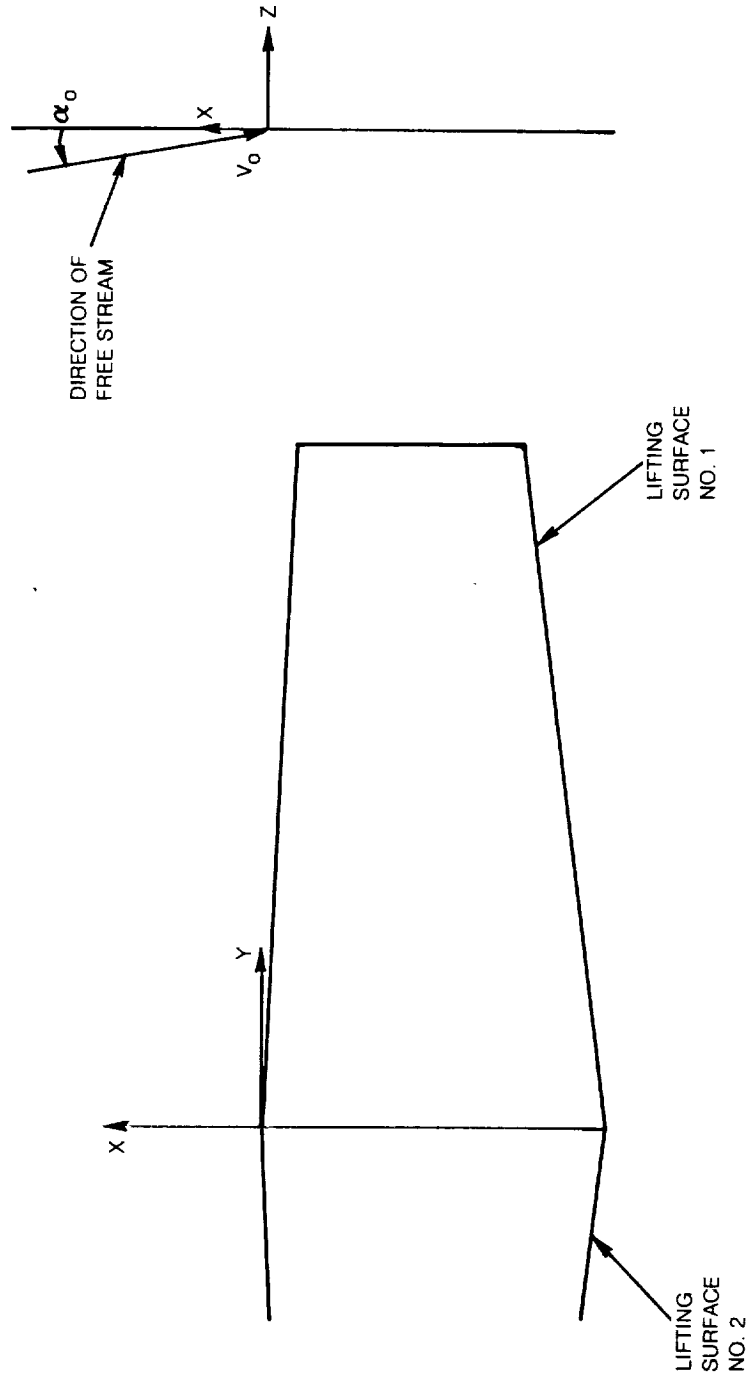
Figure 3. Wing Coordinate System

43
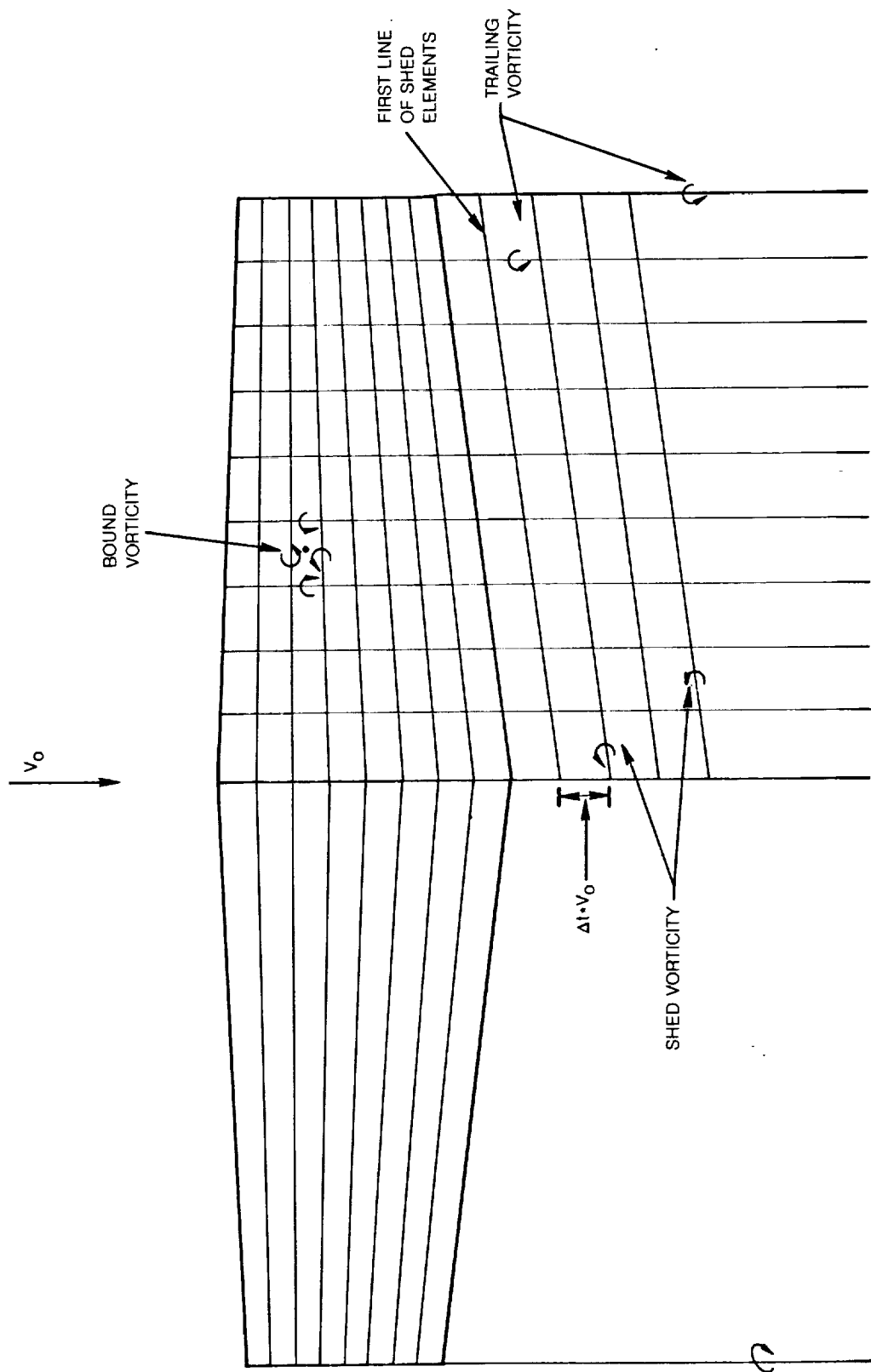
Figure 4. Modeling of Wing and Its Wake

44
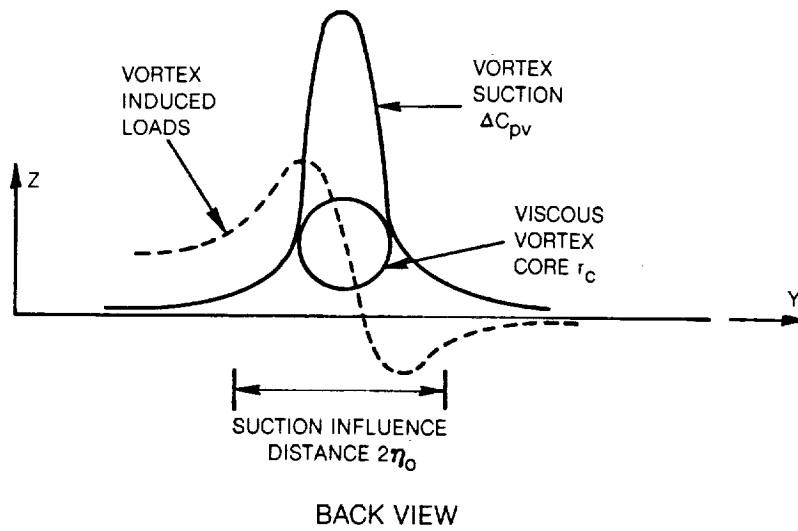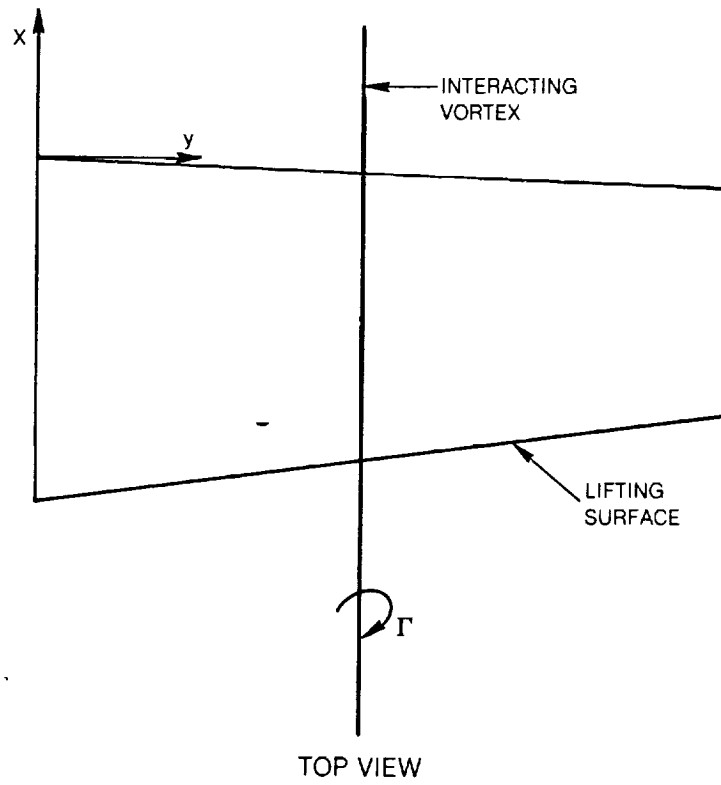
Figure 5. Simplified Model Showing Interaction Effects
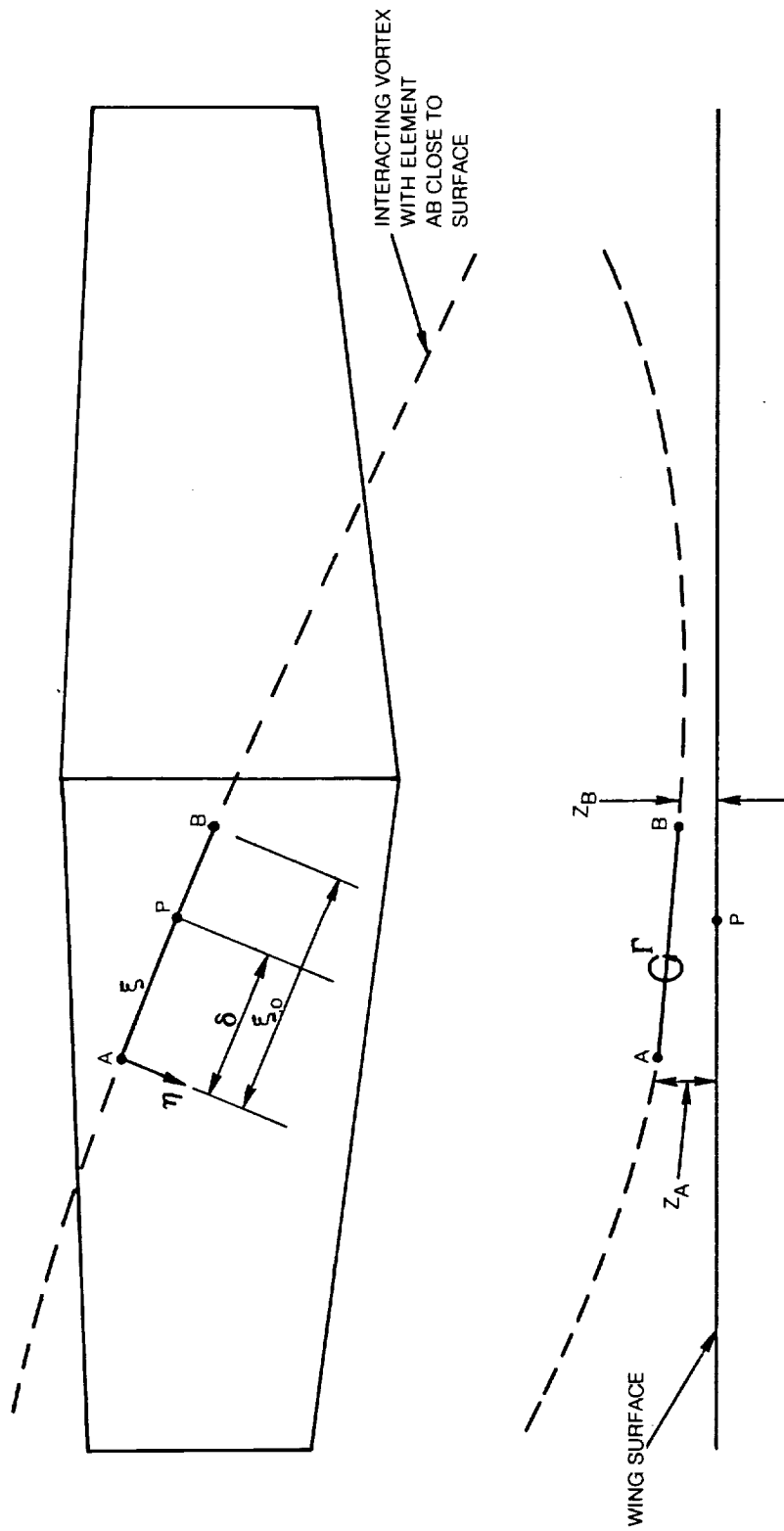
Figure 6. Modeling of Suction Effects

INTERACTING VORTEX
WITH ELEMENT
AB CLOSE TO
SURFACE

WING SURFACE

INPUT
TAIL SURFACE GEOMETRY
ANGLE OF ATTACK, a
FREE STREAM VELOCITY, v_0

FROM ROTORCRAFT WAKE
ANALYSIS FOR EACH Δ_t

w_1 INTERACTING WAKE COORDS
Γ_{w_1} CIRCULATIONS
$V_{T_1}/w_2, V_{T_1}/l_2$
(SECONDARY INDUCED EFFECTS)

ROTOR/TAIL SURFACE AERO INTERACTION MODULE

DESCRIBE TAIL SURFACE
COLLOCATION POINTS

COMPUTE GEOMETRIC
INFLUENCE COEFFS. (Aij) FOR
DOUBLET STRENGTHS

DESCRIBE PRIMARY ROTOR
WAKE ELEMENTS AT
SUBINTERVALS (Δt_2)

COMPUTE V_{T_1}/W_1 AT
EACH Δ_{t_2} USING Γ_{w_1}

COMPUTE V_{T_1}/w_2 & V_{T_1}/l_2
AT EACH Δt_2 BY INTERPOLATION

COMPUTE INFLUENCE OF TAIL
SHED AND TRAILING WAKE
ELEMENTS V_{T_2}/W_T

CALCULATE FOR EACH Δt_2
$V_T = V_{T_1}/w_1 + V_{T_1}/w_2 + V_{T_1}/l_2 +$
$V_{T_1}/W_T + V_0 \, SIN \, a$

CALCULATE PANEL DOUBLET
STRENGTHS (σ_{d_j}) BY USING NO
FLOW BOUNDARY CONDITIONS

COMPUTE LOADING AND
TRANSFER TAIL EXCITATIONS
TO VIBRATIONS PROGRAM

VIBRATORY
TAIL
EXCITATION

TO COUPLED
ROTOR/AIRFRAME
VIBRATION
ANALYSIS

ADDITIONAL NOTATION

T TAIL
I OTHER INTERFERENCE COMPONENTS

Figure 7. Flow Chart for Rotor/Tail Vibratory Excitation

INTERACTING
VORTEX

y

x

C

POINT WHERE
VORTEX IS
CUT

z

y

C

UNMODIFIED
VORTEX
GEOMETRY

MODIFIED
VORTEX
GEOMETRY
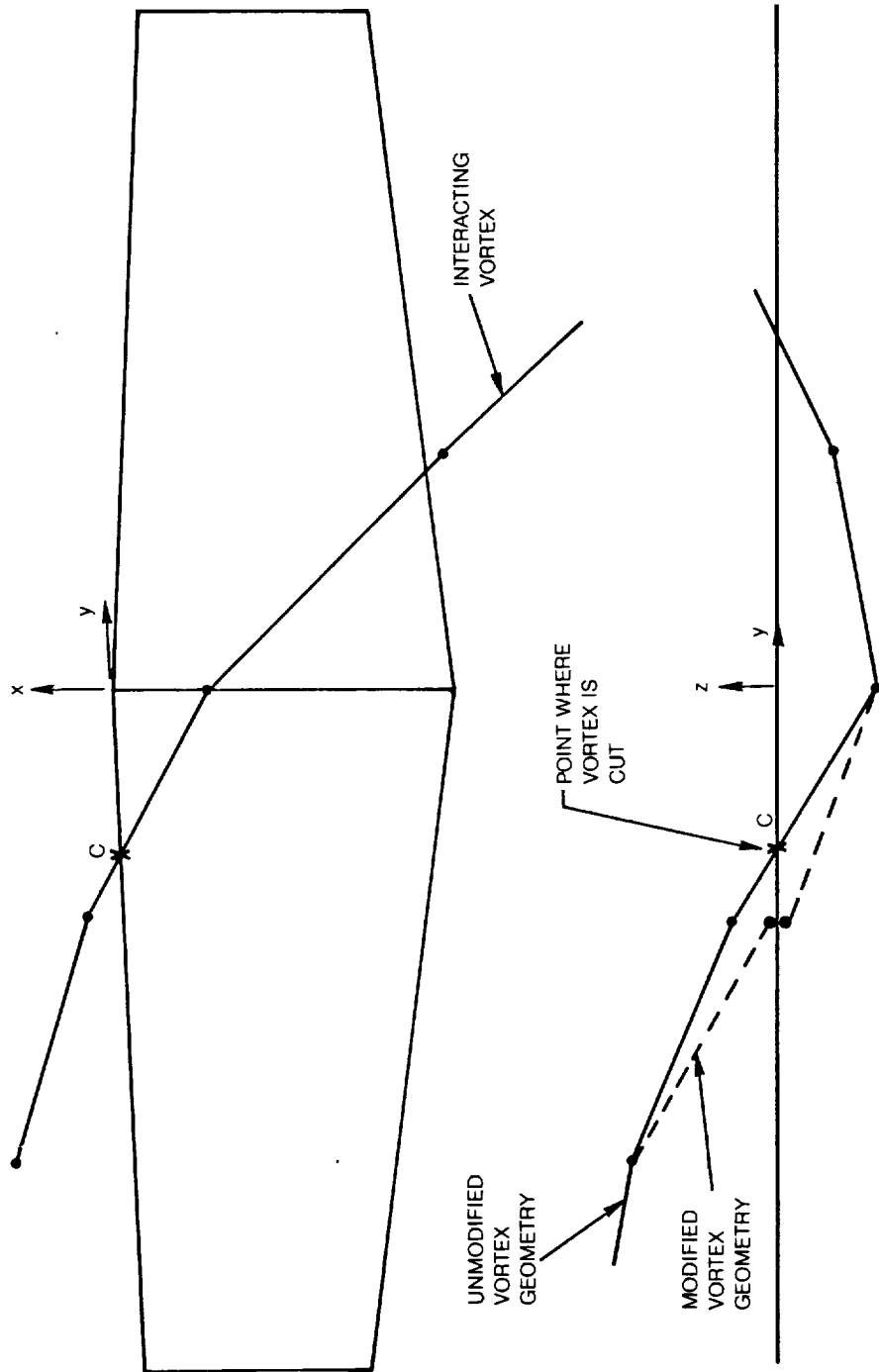
Figure 8. Vortex Geometry Modification

48
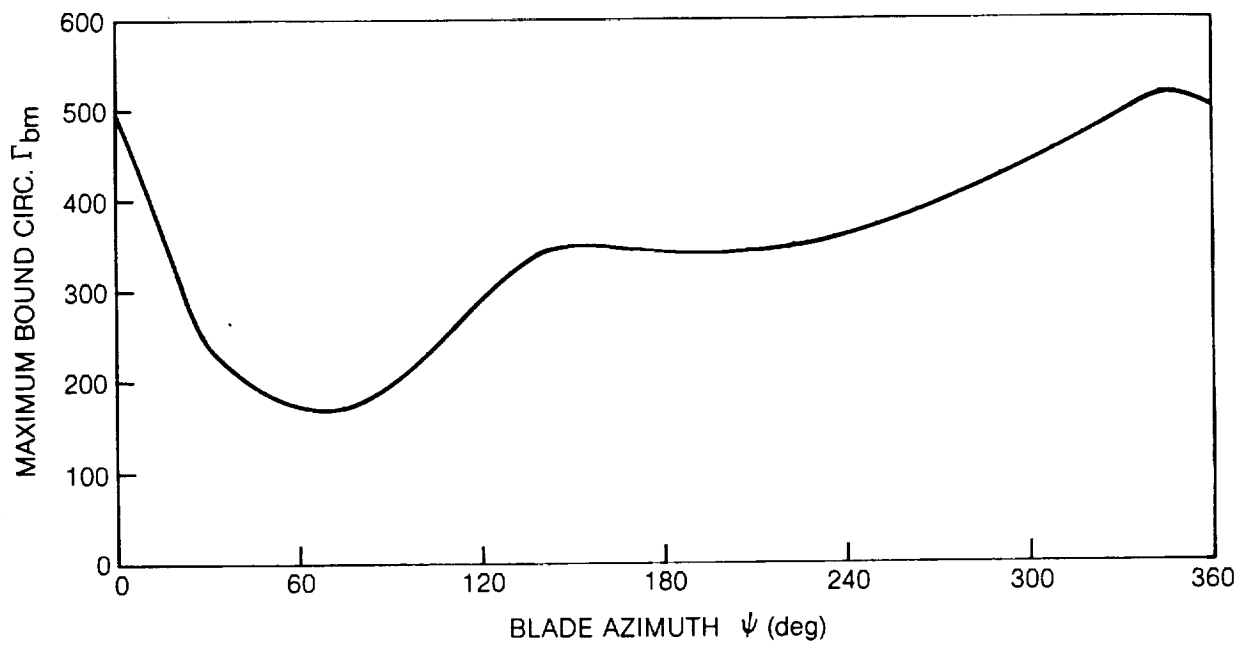
Figure 9. Maximum Γ_b Variation Around Azimuth
(feet square/sec)

PART OF FAR-WAKE
INTERACTING ELEMENTS
BOUNDARY BETWEEN THE TWO PARTS

STABLIZER

BLADE

30°

HUB

TOP VIEW
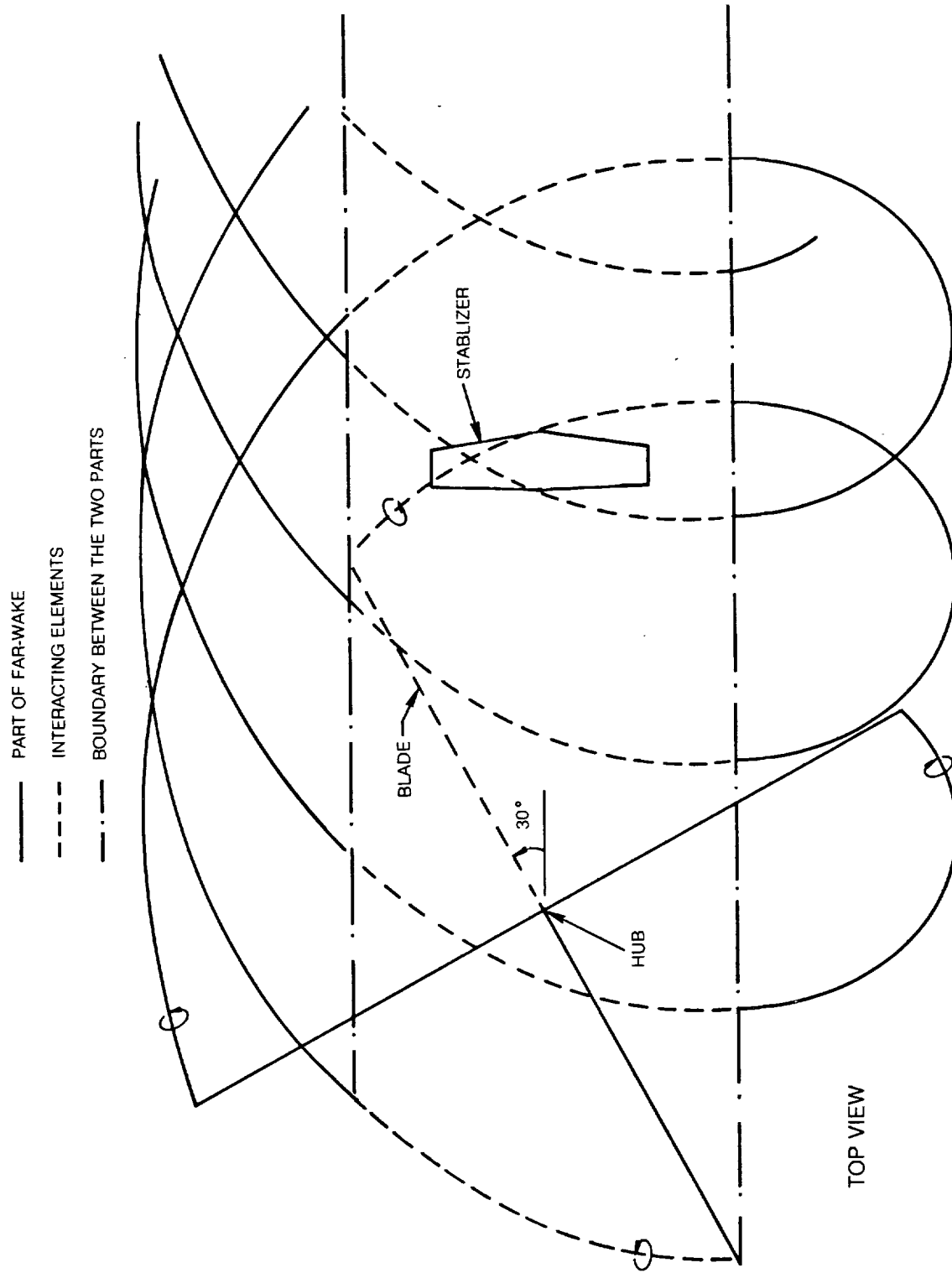
Figure 10. An Example of Splitting of Rotor Wake Into Two Parts
$\mu = 0.4$, Only Tip Vortices Shown for $\psi = 30$ deg

50
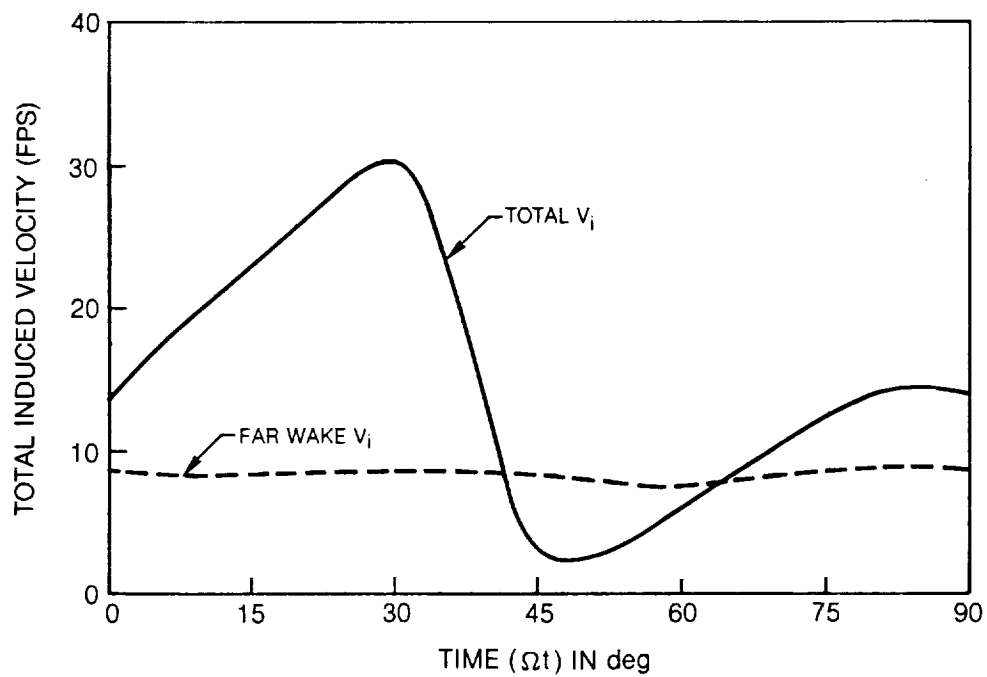
**Figure 11. Variation of Induced Velocity at Stablizier
(At Quarter Chord Point on Wing Centerline)**
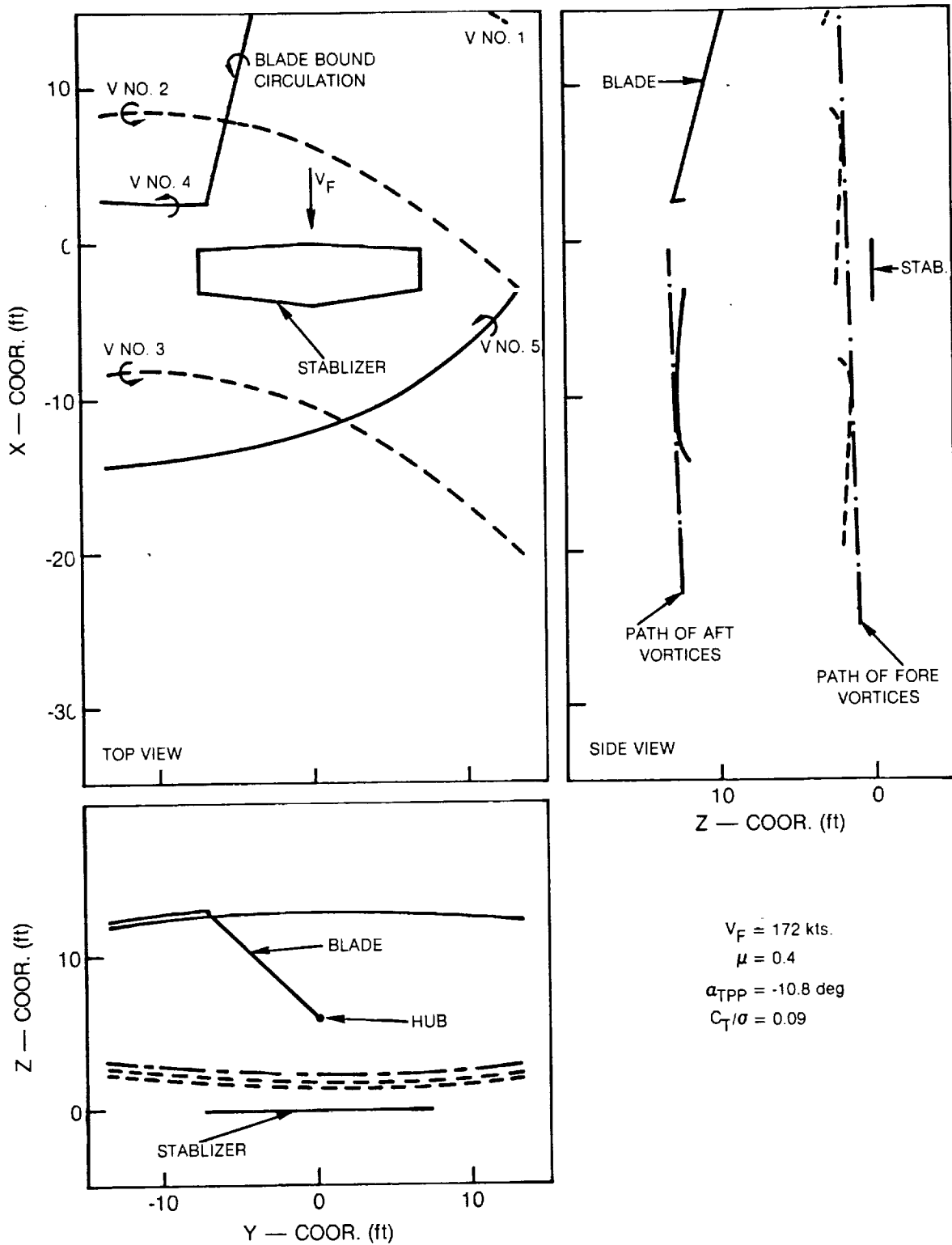
Figure 12. Vortex Geometry at Step No. 1

52
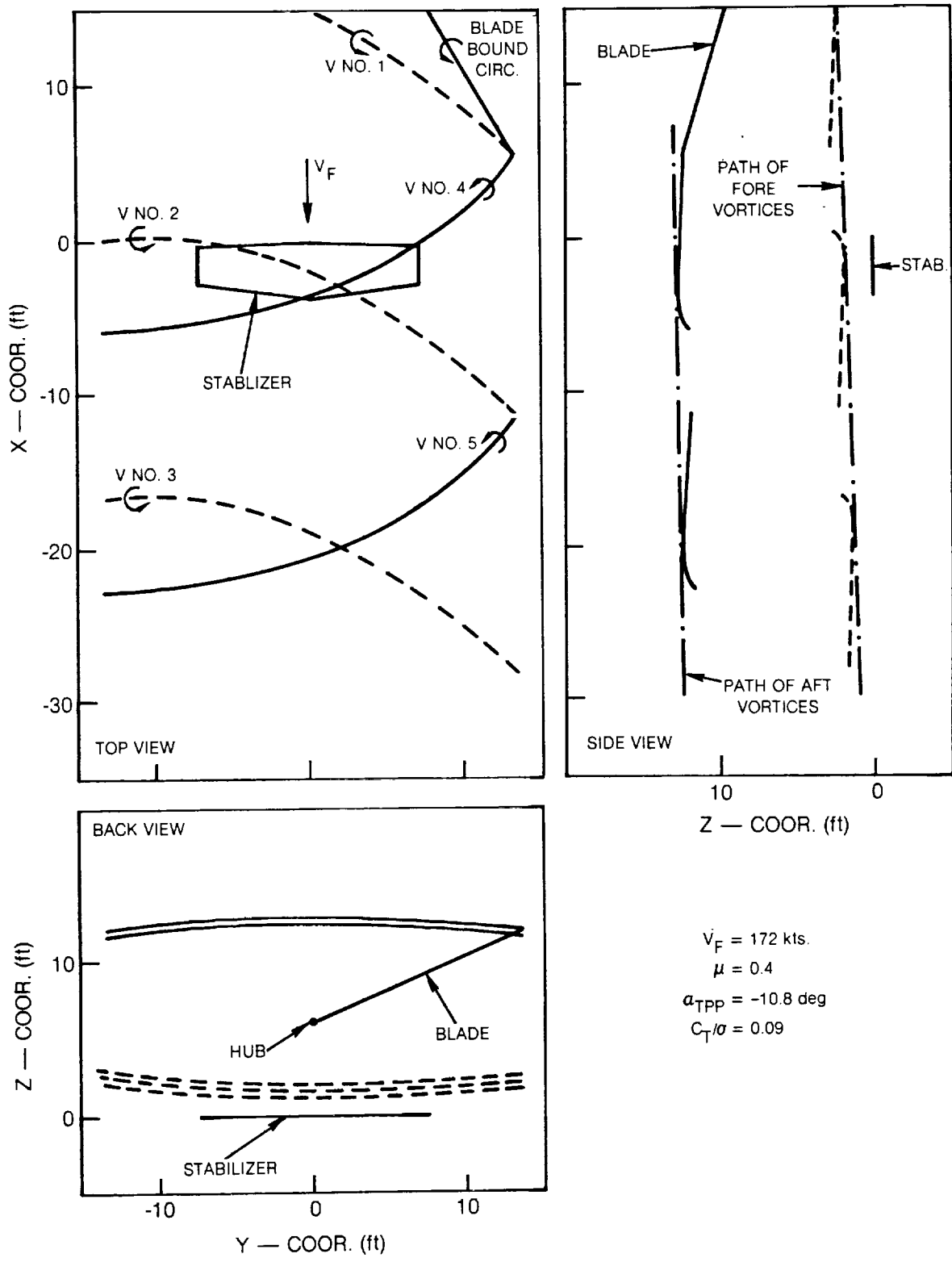
Figure 13. Vortex Geometry at Step No. 7
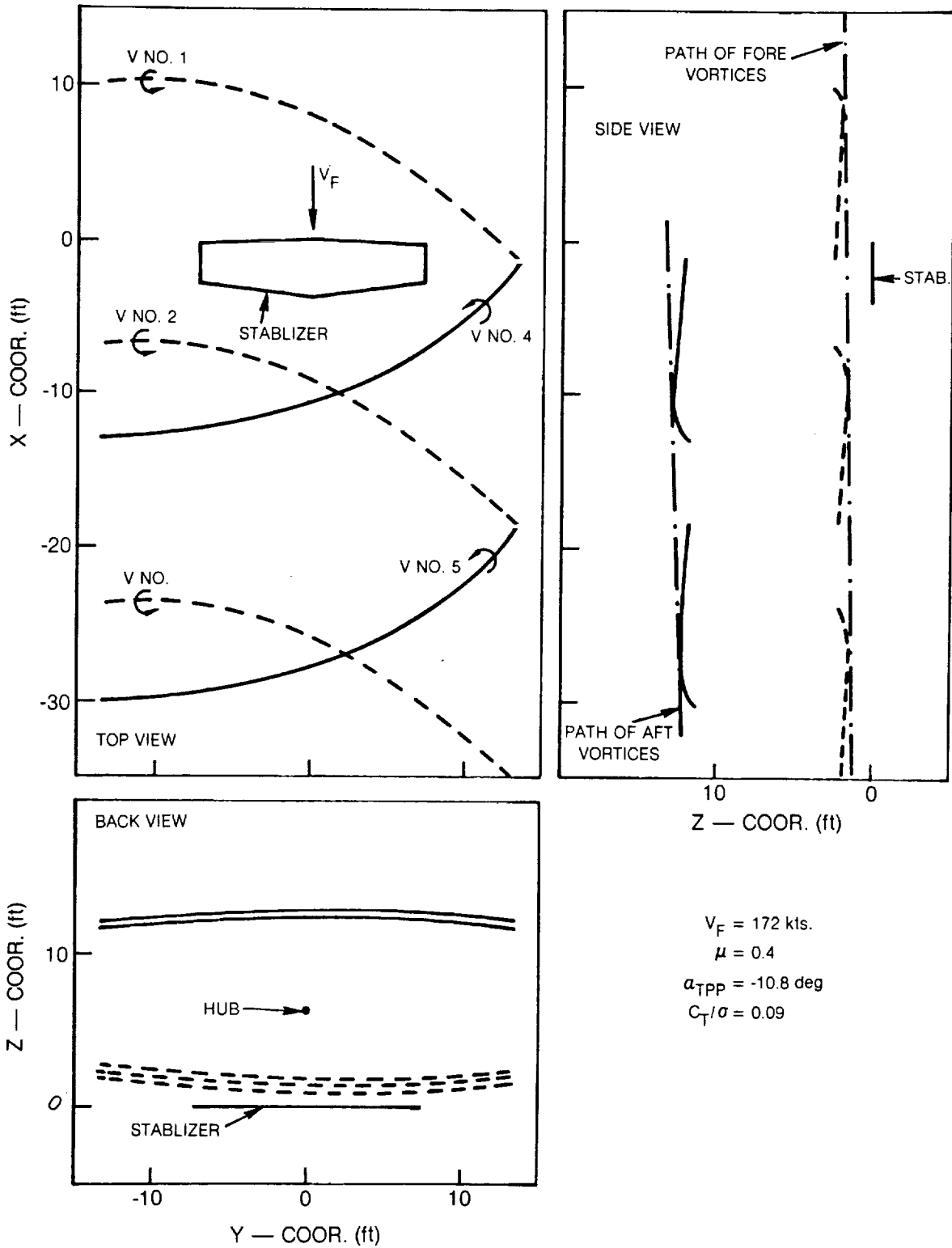
Figure 14. Vortex Geometry at Step No. 12

The figure contains several views labeled TOP VIEW, SIDE VIEW, and BACK VIEW.

TOP VIEW (X — COOR. (ft) vs. axis):
- V NO. 1
- V NO. 2
- V NO. (3)
- V NO. 4
- V NO. 5
- V_F
- STABLIZER

SIDE VIEW (Z — COOR. (ft)):
- PATH OF FORE VORTICES
- STAB.
- PATH OF AFT VORTICES

BACK VIEW (Z — COOR. (ft) vs. Y — COOR. (ft)):
- HUB
- STABLIZER

V_F = 172 kts.

μ = 0.4

a_{TPP} = -10.8 deg

C_T/σ = 0.09

54
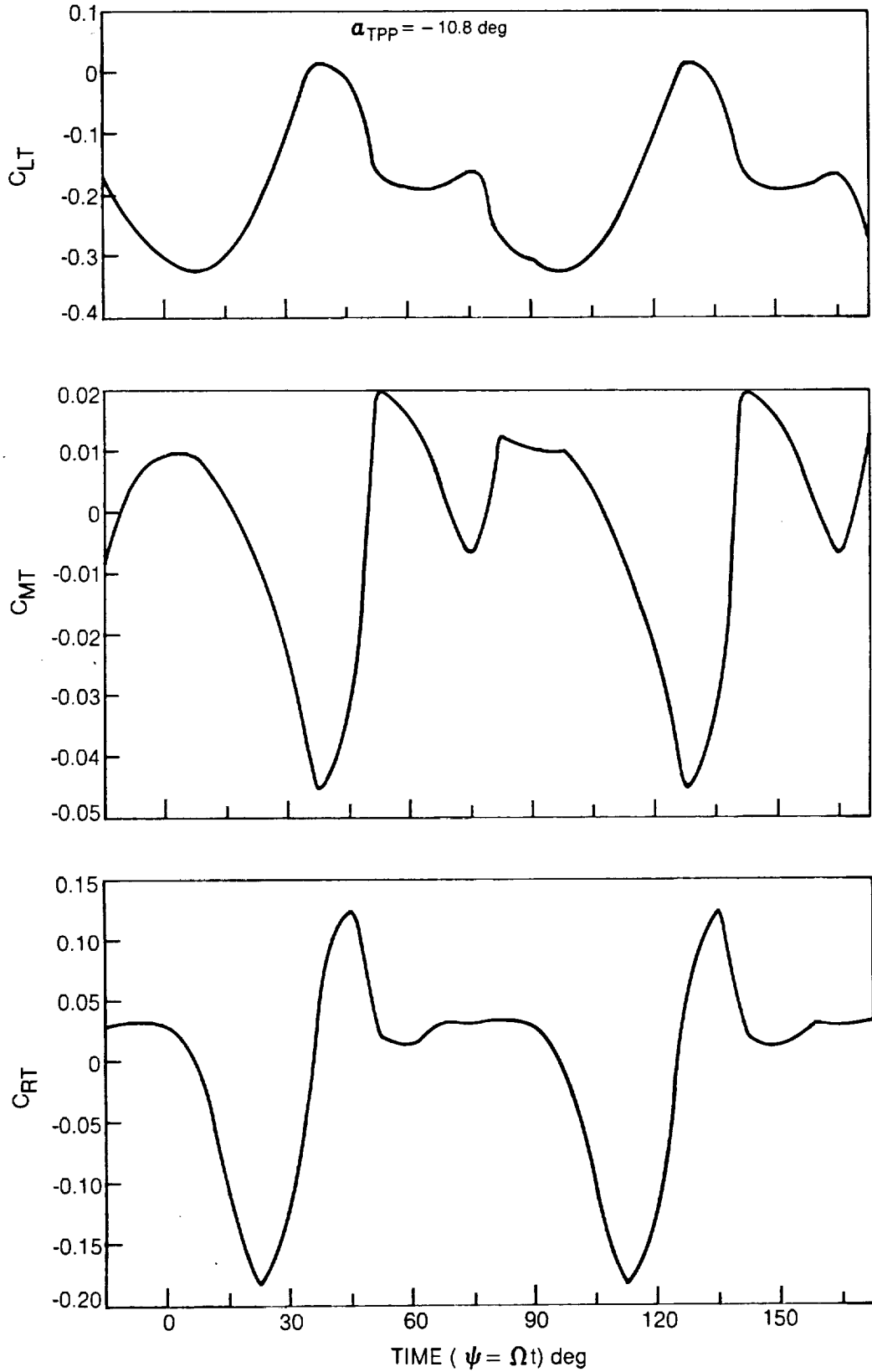
Figure 15. Stabilizer Airloads Time History
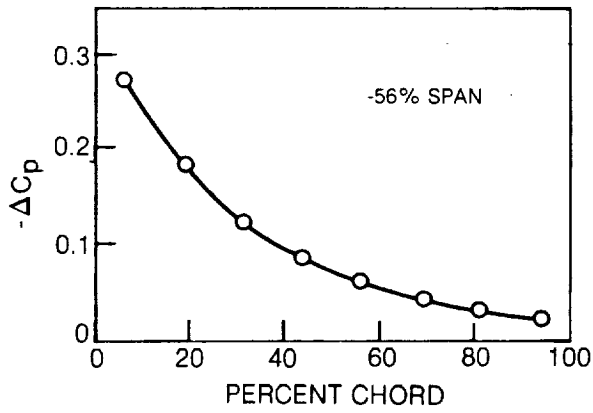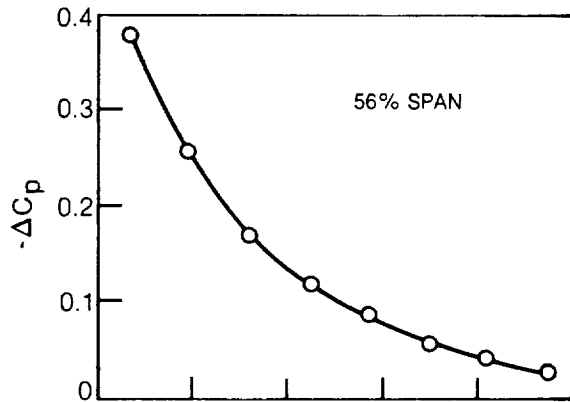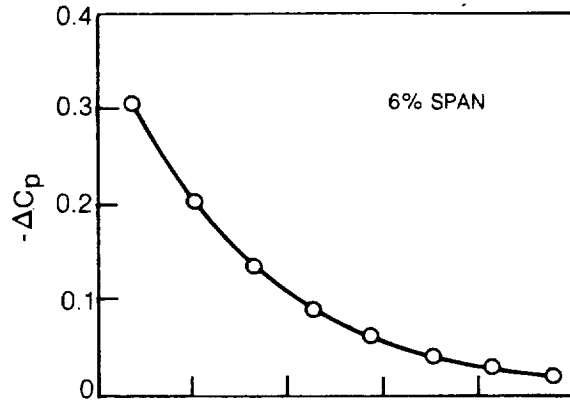
Figure 16. Chordwise Airload Variation at Step No. 1
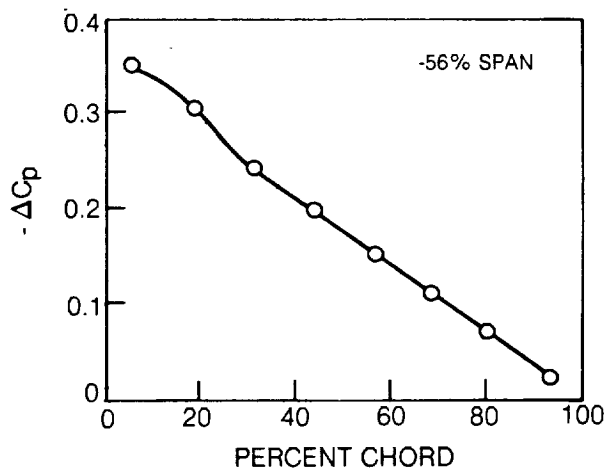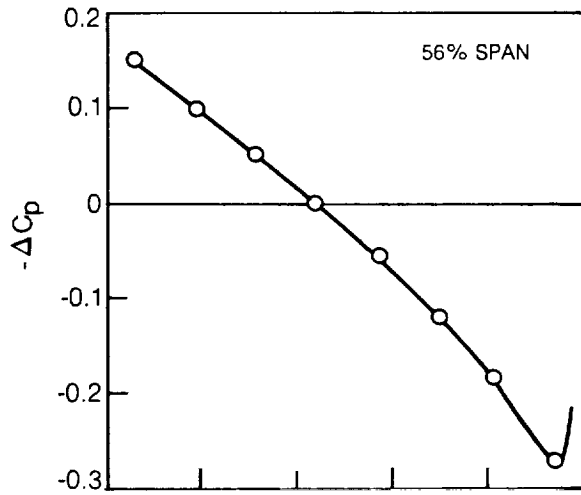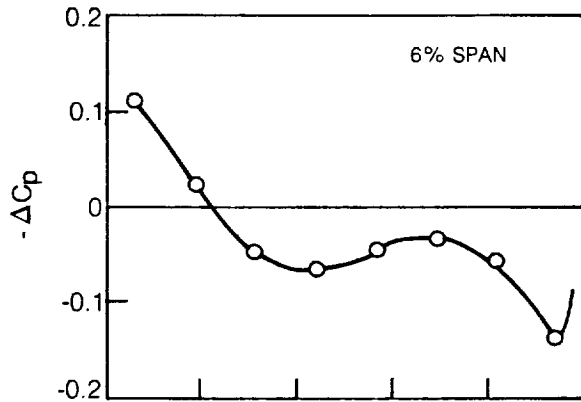
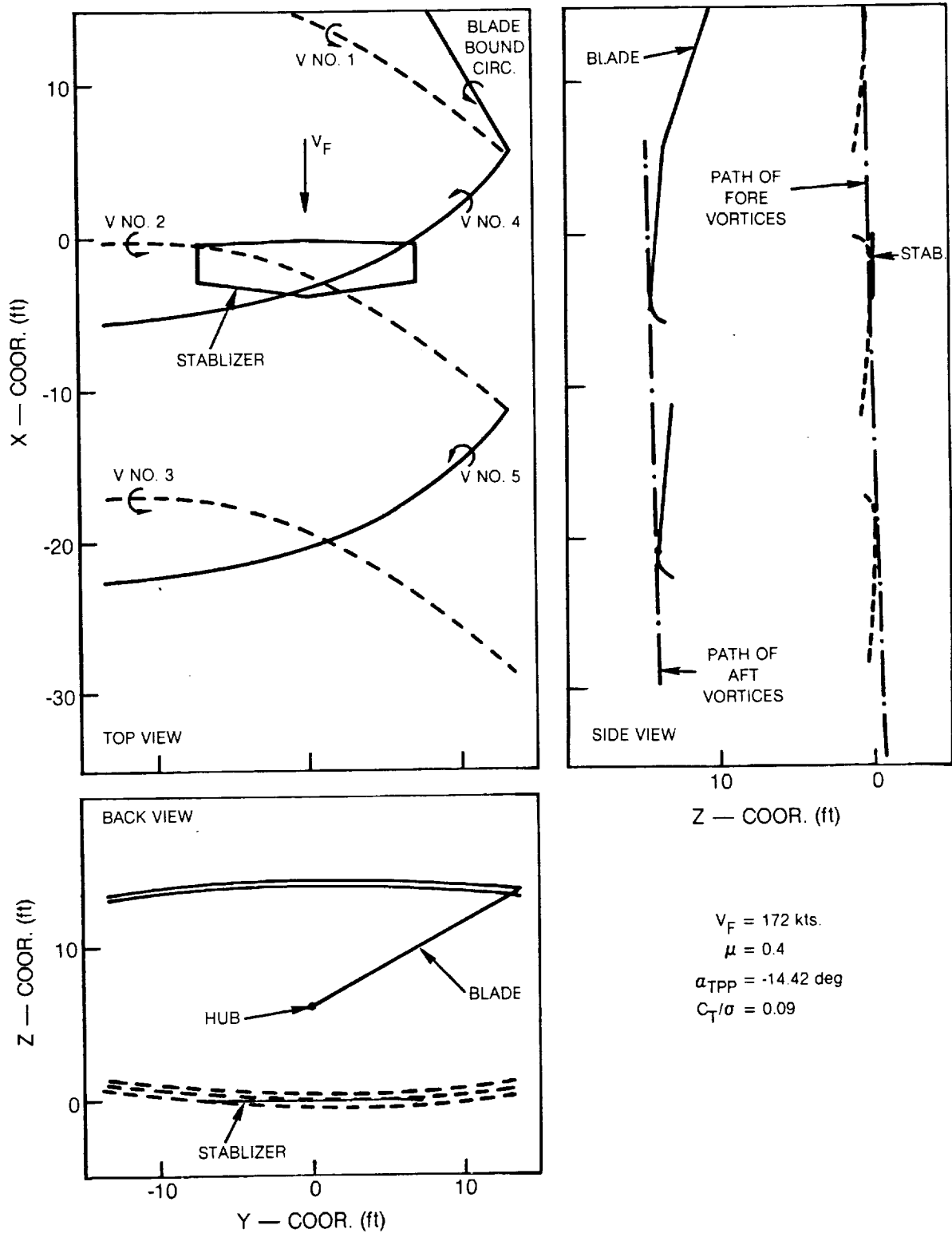**Figure 17. Chordwise Airload Variation at Step No. 7**
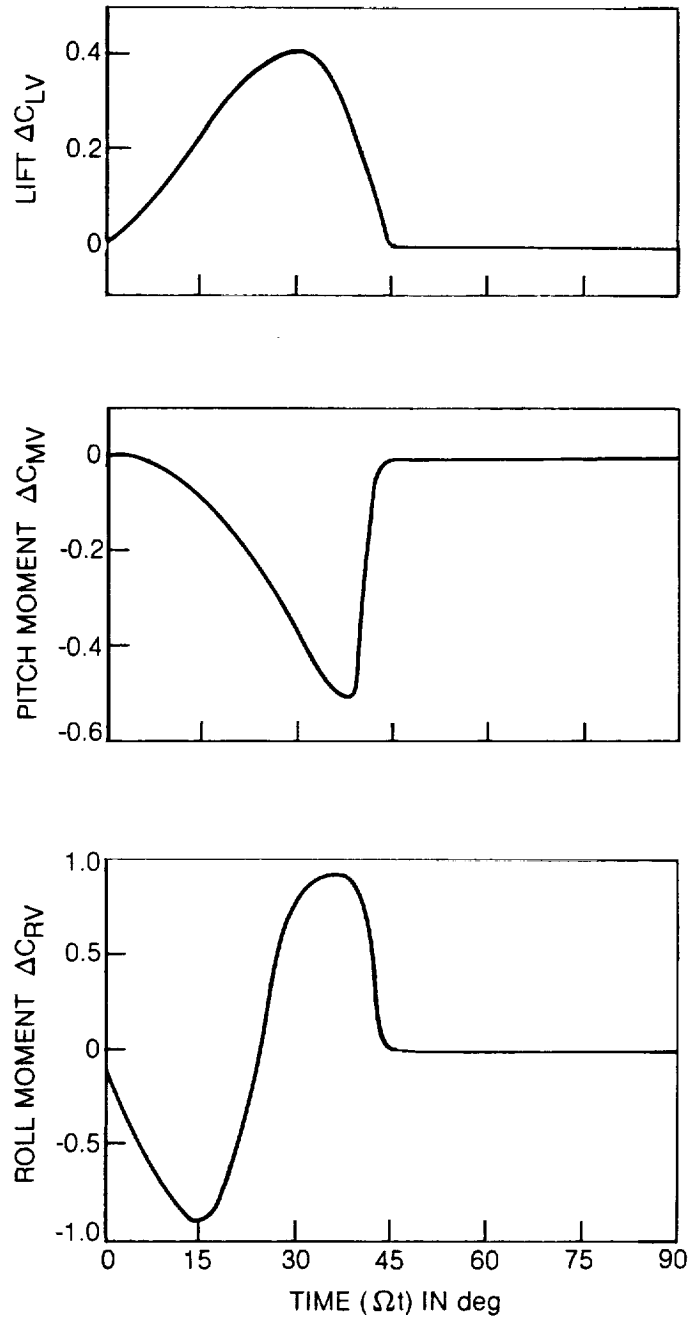
Figure 18. Vortex Geometry at Step No. 7

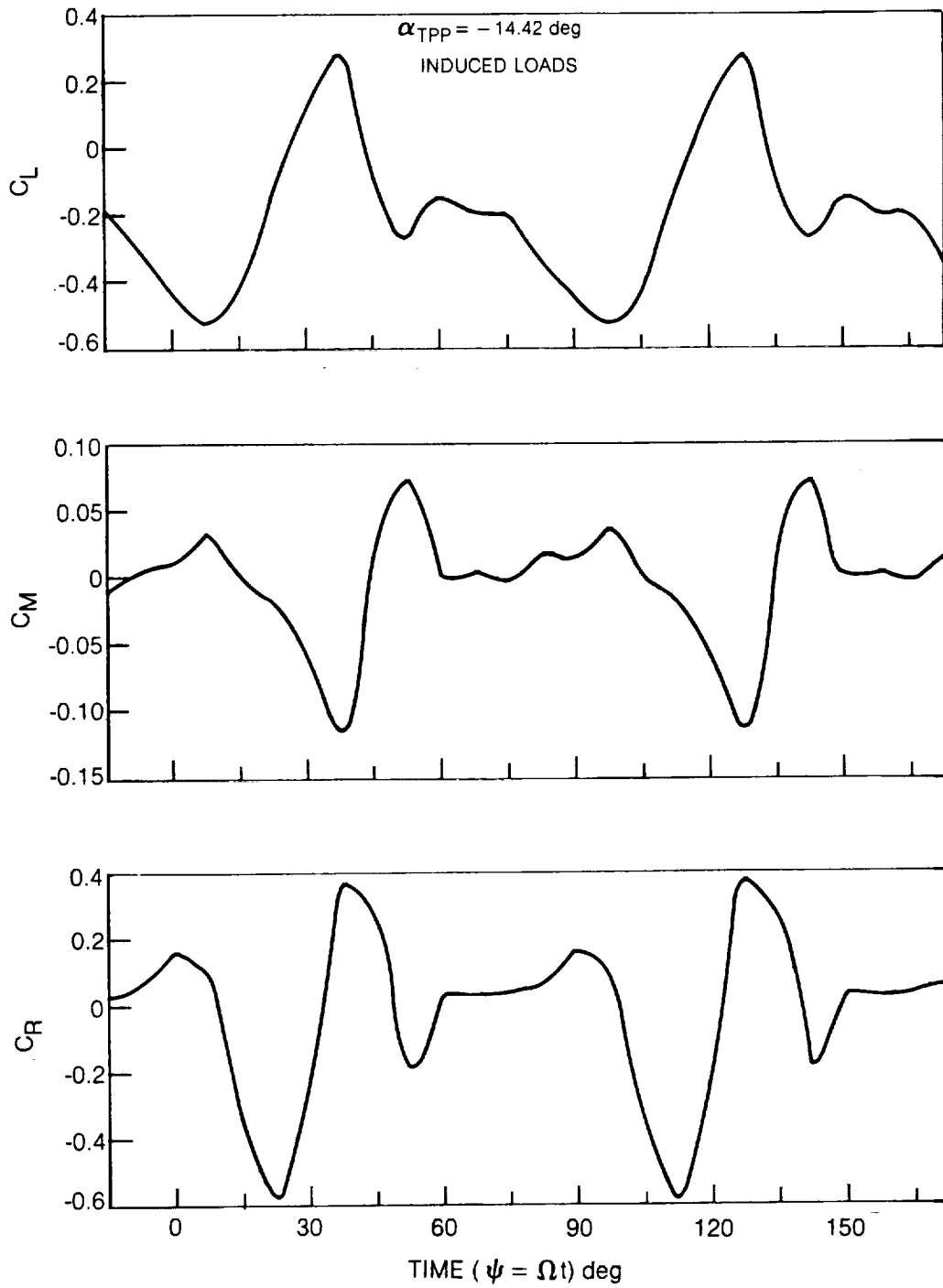Figure 19. Nonlinear Suction Airloads

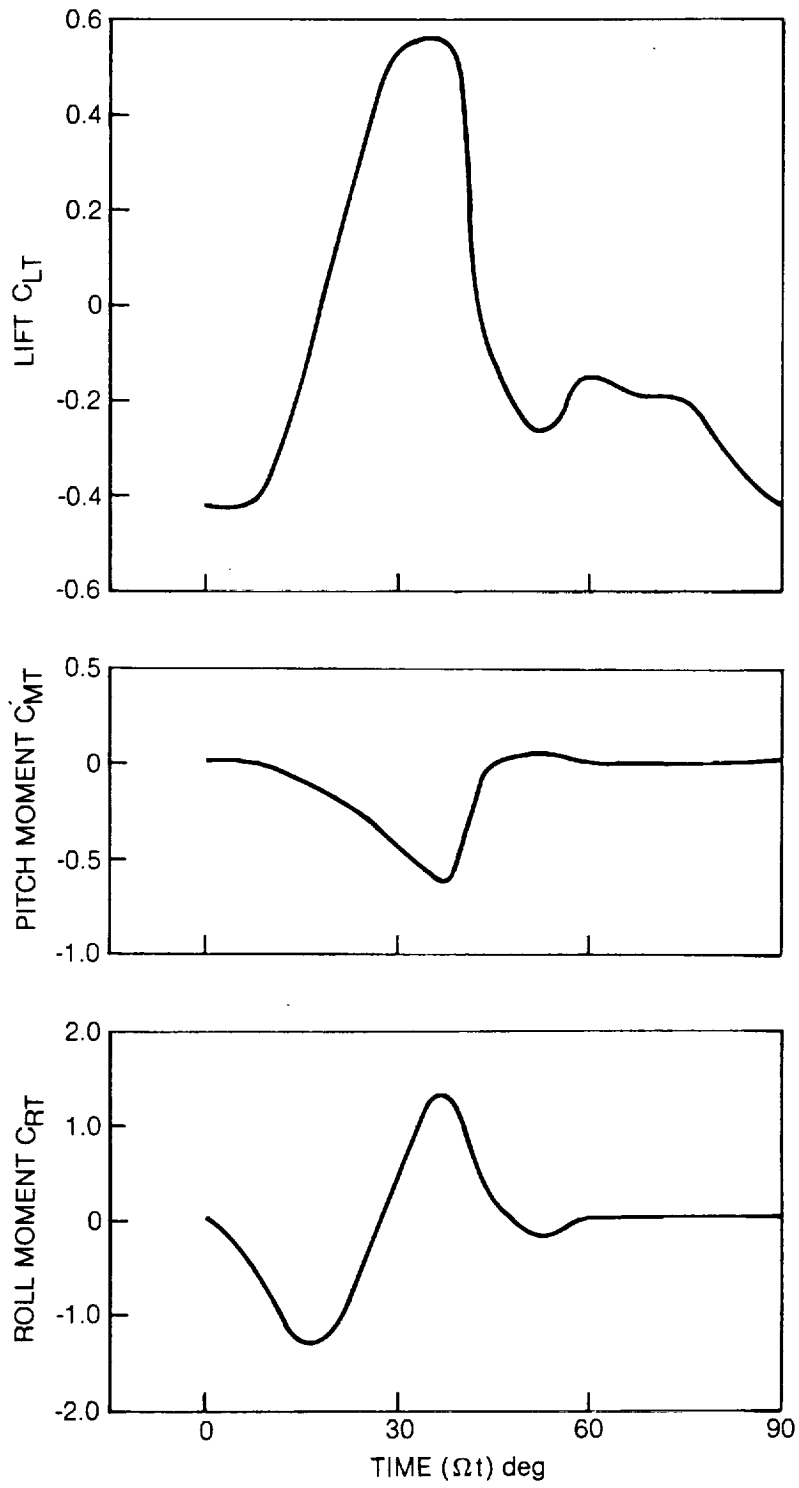**Figure 20. Stabilizer Airloads Time History**

Figure 21. Variation of Total Loads Over One Blade Passage $\alpha_{TPP} = -14.42$ deg

1. Report No. NASA CR-165893	2. Government Accession No.	3. Recipient's Catalog No.
4. Title and Subtitle A DOUBLET LATTICE METHOD FOR THE DETERMINATION OF ROTOR INDUCED EMPENNAGE VIBRATION AIRLOADS - ANALYSIS DESCRIPTION AND PROGRAM DOCUMENTATION		5. Report Date June 1982
		6. Performing Organization Code
7. Author(s) Santu T. Gangwani		8. Performing Organization Report No. UTRC81-7
		10. Work Unit No.
9. Performing Organization Name and Address United Technologies Research Center Silver Lane East Hartford, CT 06108		
		11. Contract or Grant No. NAS1-16058
12. Sponsoring Agency Name and Address NASA Langley Research Center Hampton, VA 23665		13. Type of Report and Period Covered Contractor Report
		14. Sponsoring Agency Code

15. Supplementary Notes

16. Abstract

An efficient state-of-the-art method has been developed to determine the unsteady vibratory airloads produced by the interaction of the main rotor wake with a helicopter empennage. This method has been incorporated into a computer program, Rotor Induced Empennage Vibration Analysis (RIEVA). The program requires the main rotor wake position and the strength of the vortices locates near the empennage surfaces. A nonlinear lifting surface analysis is utilized to predict the aerodynamic loads on the empennage surfaces in the presence of these concentrated vortices. The analysis has been formulated to include all pertinent effects such as suction of the interacting vortices and the shed vorticity behind the empennage surfaces. The analysis employs a time domain solution. The output of the program consists of chordwise and spanwise airload distributions on the empennage surfaces. The airload distributions are harmonically analyzed and formulated for input into the Coupled Rotor/Airframe Vibration Analysis.

17. Key Words (Suggested by Author(s)) Empennage Rotor wake Vibratory Unsteady Airloads	18. Distribution Statement Unlimited - Unclassified		
19. Security Classif. (of this report) Unclassified	20. Security Classif. (of this page) Unclassified	21. No. of Pages 61	22. Price